Structure of the human TIP60-C histone exchange and acetyltransferase complex

Changqing Li, Ekaterina Smirnova, Charlotte Schnitzler, Corinne Crucifix, Alice Brion, Arnaud Poterszman, Patrick Schultz, Gabor Papai, Adam Ben-Shem, Jean-Paul Concordet

Article

Structure of the human TIP60-C histone exchange and acetyltransferase complex

https://doi.org/10.1038/s41586-024-08011-w

Received: 22 November 2023

Accepted: 3 September 2024

Published online: 11 September 2024

Open access

Check for updates

Changqing Li[1,2,3,4], Ekaterina Smirnova[1,2,3,4], Charlotte Schnitzler[1,2,3,4], Corinne Crucifix[1,2,3,4], Jean Paul Concordet[5], Alice Brion[5], Arnaud Poterszman[1,2,3,4], Patrick Schultz[1,2,3,4], Gabor Papai[1,2,3,4] & Adam Ben-Shem[1,2,3,4] ✉

Chromatin structure is a key regulator of DNA transcription, replication and repair[1]. In humans, the TIP60–EP400 complex (TIP60-C) is a 20-subunit assembly that affects chromatin structure through two enzymatic activities: ATP-dependent exchange of histone H2A–H2B for H2A.Z–H2B, and histone acetylation. In yeast, however, these activities are performed by two independent complexes—SWR1 and NuA4, respectively[2,3]. How the activities of the two complexes are merged into one supercomplex in humans, and what this association entails for the structure and mechanism of the proteins and their recruitment to chromatin, are unknown. Here we describe the structure of the endogenous human TIP60-C. We find a three-lobed architecture composed of SWR1-like (SWR1L) and NuA4-like (NuA4L) parts, which associate with a TRRAP activator-binding module. The huge EP400 subunit contains the ATPase motor, traverses the junction between SWR1L and NuA4L twice and constitutes the scaffold of the three-lobed architecture. NuA4L is completely rearranged compared with its yeast counterpart. TRRAP is flexibly tethered to NuA4L—in stark contrast to its robust connection to the completely opposite side of NuA4 in yeast[4–7]. A modelled nucleosome bound to SWR1L, supported by tests of TIP60-C activity, suggests that some aspects of the histone exchange mechanism diverge from what is seen in yeast[8,9]. Furthermore, a fixed actin module (as opposed to the mobile actin subcomplex in SWR1; ref. 8), the flexibility of TRRAP and the weak effect of extranucleosomal DNA on exchange activity lead to a different, activator-based mode of enlisting TIP60-C to chromatin.

Chromatin structure regulates all DNA transactions, including transcription, replication and repair. The nucleosome, composed of 146 base pairs (bp) of DNA wrapped around a histone octamer, constitutes the repeated chromatin unit. Histone variants that deviate in sequence from the canonical ones and post-translational modification of histones can either directly alter chromatin structure or recruit proteins to achieve that effect[10]. Human TIP60-C is a 1.8-MDa complex, composed of at least 20 subunits, that has two chromatin-modifying enzymatic activities: acetylation of histones H4 and H2A; and incorporation, driven by an ATPase situated in subunit EP400, of the histone variant H2A.Z instead of the canonical H2A[2,11]. Histone acetylation by TIP60-C is associated with active gene expression[12] as well as the repair of DNA double-strand breaks[13]. H2A.Z is an essential, conserved histone variant enriched in nucleosomes flanking the transcription start site, but its role is perplexing because it seems to foster transcriptional activation of some genes but repression of others[14,15]. The molecular mechanism that underlies the contradictory effects of H2A.Z is poorly understood.

In yeast, these chromatin modifications are performed by two separate multiprotein assemblies: the SWR1 complex introduces the yeast homologue of H2A.Z, Htz1, into nucleosomes by ATP-dependent exchange of H2A–H2B histone dimers for Htz1–H2B; and the NuA4 complex carries out the histone acetyltransferase activity (Extended Data Fig. 1). The yeast complexes are believed to act sequentially in a coordinated manner, and their human analogues are both incorporated into TIP60-C. Structures of the yeast NuA4 and SWR1 complexes have been resolved by single-particle cryo-electron microscopy (cryo-EM)[4–8], but how these two activities physically merge in human TIP60-C and what this association entails are unknown. Here we present the 2.4–3.3 Å resolution cryo-EM structure of endogenous TIP60-C purified from human cells. We complement the structure with a set of biochemical tests to reveal its implications for the functional properties, mechanism of action and recruitment to chromatin of TIP60-C. On the basis of these results, we propose new perspectives for the outcome of H2A.Z deposition. We thus provide a molecular framework for understanding the activity of TIP60-C in DNA repair and transcription regulation as well as its function in human diseases. Indeed, synthetic lethality between TIP60-C and the SWI/SNF family of chromatin remodellers in human cancer cell lines suggests that inhibiting TIP60-C is an attractive

[1]Université de Strasbourg, Institut de Génétique et de Biologie Moléculaire et Cellulaire (IGBMC) UMR 7104 UMR S 1258, Illkirch, France. [2]CNRS, UMR 7104, Illkirch, France. [3]Inserm, UMR S 1258, Illkirch, France. [4]Equipe Labellisée Ligue Contre le Cancer, Institut de Génétique et de Biologie Moléculaire et Cellulaire (IGBMC), Illkirch, France. [5]Museum National d'Histoire Naturelle, U 1154 Inserm UMR 7196 CNRS, Paris, France. ✉e-mail: adam@igbmc.fr

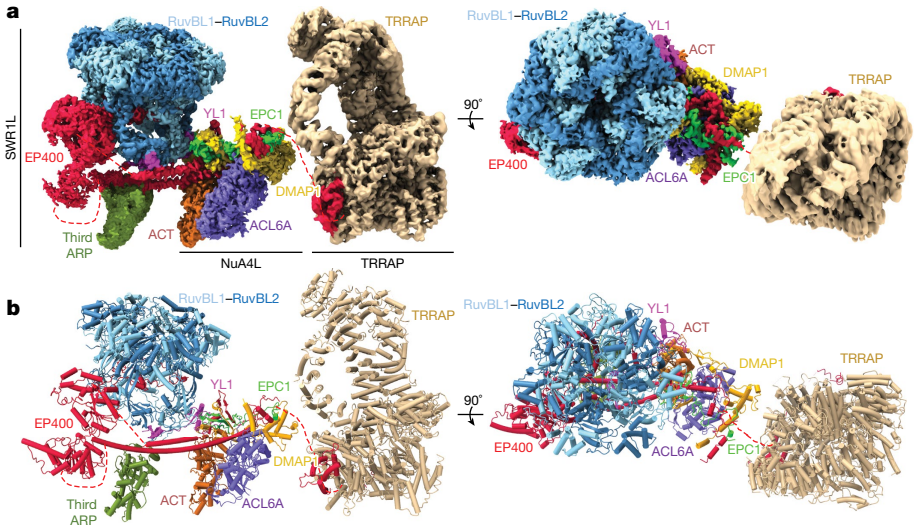

Fig. 1 | Architecture of the human TIP60–EP400 complex (TIP60-C). a, Two views of the composite cryo-EM map of endogenous human TIP60-C. **b**, Corresponding views of the atomic model of TIP60-C. Colours of subunits in maps and models match the colours of their written names. Dashed lines represent physical connections that are not visible in the maps. ACT, actin.

therapeutic approach for the many cancer types in which SWI/SNF is perturbed[16].

Overall structure of TIP60-C

To isolate endogenous TIP60-C, we used CRISPR–Cas9 technology to fuse an SBP-3×Flag affinity tag at the C terminus of subunit EPC1 in human erythroleukaemic K562 cells. The purified complex contained all expected subunits (Extended Data Fig. 2a,b) and included an H2A.Z–H2B dimer in near stoichiometric amounts. The complex was subjected to single-particle cryo-EM analysis (Extended Data Figs. 2c, 3a,d,f, 4, 5 and 6a and Extended Data Table 1). Notably, we find that the density map of TIP60-C is composed of three large subcomplexes instead of the expected two (Fig. 1a). The SWR1L subcomplex is dominated by a hetero-hexameric core of the RuvBL1 and RuvBL2 subunits as found in yeast[8] (Fig. 1b). The C-lobe of the EP400 ATPase domain is bound to the hexamer, and projects a large extended insertion into it. The Swc6–Arp6 dimer that appears in yeast at the hexamer face opposing the ATPase C-lobe is absent in TIP60-C, whereas an isolated ARP (actin-related protein) is located beneath the hexamer base, where no protein occurs in yeast. The second subcomplex, reminiscent of the NuA4 core, is markedly diminished and rearranged with respect to the yeast version (Fig. 1b). In particular, a large robust neck domain in yeast serves to strongly couple the TRRAP homologue, Tra1, to the actin module at the core of NuA4. In TIP60-C, the actin module, which comprises two ARPs (actin and actin-like protein 6A (ACL6A)), the DMAP1 subunit and the N-terminal part of the helicase-SANT-associated (HSA) helix, sits on top of a highly dwindled small neck that shows very little resemblance to its yeast counterpart. Furthermore, as a result of the loss of a massive neck domain in TIP60-C, the 400-kDa TRRAP subunit is not tightly associated with NuA4L, but instead constitutes a separate semi-autonomous third subcomplex located on the opposite side of NuA4L when compared to yeast. Owing to this flexibility, our map of TIP60-C does not resolve TRRAP well, and it appears as a large cloud of density of roughly the expected size, next to the degenerate neck domain (Extended Data Fig. 3d). To investigate our interpretation of this cloud as a highly mobile TRRAP, we reconstituted a three-dimensional (3D) map of the holo-complex from negatively stained molecules. Three-dimensional classification clearly shows a very large density in different orientations around the neck (Extended Data Fig. 3b,c). The more populated of these classes show clear structural features of TRRAP, which could be fitted well into the maps (Extended Data Fig. 3e). Moreover, by focusing our image analysis on TRRAP, we could solve the structure of this subcomplex by itself (Fig. 1). We find that the SANT (Swi3–Ada–NCoR–TFIIIB) domain of subunit EP400 strongly associates with TRRAP, thus establishing that TRRAP is part of the holo-complex and is connected to the NuA4L core through an 83-residue, unfolded loop that lies between the SANT domain and the part of EP400 embedded in the NuA4L core. Next to the SANT domain we find a poorly resolved additional large density, the shape of which fits that of the KAT (lysine acetyltransferase) module (Extended Data Fig. 6b–e). The maps of TRRAP and holo-TIP60 do not reveal a density that can unambiguously be attributed to the KAT module. This is probably a direct result of the module's high mobility, which is afforded by its tethering to NuA4L through a long, unstructured EPC1 linker of around 100 amino acids, as was found in NuA4 in yeast[4]. Conformational analysis of the TRRAP module identified a fraction of the particle population with a density next to the EP400 SANT domain, into which the KAT module could be fitted (Extended Data Fig. 6b,c). We thus hypothesized that this density corresponds to the KAT module, which, in a fraction of TIP60-C particles, physically associates with TRRAP or the SANT domain. Such an interaction has been detected previously and has been shown to occur and to regulate KAT activity in vivo[17]. As for yeast NuA4, a few subunits are not detected in the density maps because they are flexibly bound to the core. These are YEATS4 and the TINTIN module, which 'read' different histone post-translational modifications. TRRAP, or its yeast homologue Tra1, serves as a docking platform for activators that recruit complexes to specific chromatin loci[18]. In SAGA and yeast NuA4, in which TRRAP (Tra1) is firmly coupled to the core, the enzymatic modules have been endowed with inherent flexibility to reach their targets[4]. By contrast, the TIP60-C ATPase lacks such dynamics, and a rigid TRRAP would entail a fixed distance between the activator platform subunit and the active site of the ATPase. This would leave no leeway for the ATPase to search for its target nucleosome, apart from the flexibility afforded by the activation domain of the recruiting transcription factor, which can be minimal. It stands to reason, therefore, that TRRAP flexibility allows for target searching by SWR1L.

Connecting the subcomplexes

The structure of TIP60-C reveals that the two enzymatic parts, SWR1L and NuA4L, are firmly connected through several bridging elements. The N-terminal domain of the YL1/VPS72 subunit holds the H2A.Z–H2B dimer before its deposition into the nucleosome (Fig. 2a). More to its C terminus, a long and extended region presenting a β-sheet interacts with and intercalates between two protomers of the RuvBL1–RuvBL2 hexamer (Fig. 2b,c). This extended region then crosses the entire SWR1L part, to be followed by an additional compact domain (residues 290–355) that is not observed in yeast SWR1 and comprises a helix, a β-sheet with two strands and several structured loops.

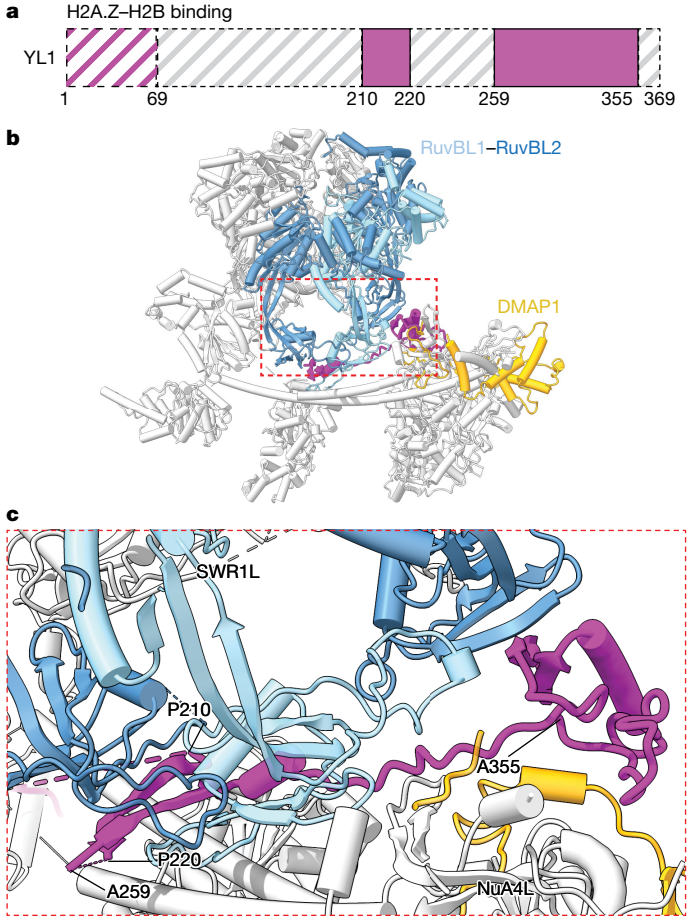

Fig. 2 | YL1 glues SWR1L to NuA4L. a, Domain organization of YL1. The domain boundaries are marked with residue numbers. The magenta parts represent the modelled domains. **b**, Location of YL1 within TIP60-C. **c**, Enlarged view of the boxed area showing the interaction of YL1 with both SWR1L and NuA4L.

This compact YL1 domain at the periphery of the supercomplex acts as a glue that connects the SWR1L and NuA4L parts. One face of this YL1 domain packs against a β-sheet from the base of a protomer in the RuvBL1–RuvBL2 hexamer, whereas its opposite face binds to a loop and a helix from the DMAP1 subunit, which is a component of NuA4L where it envelopes the actin module.

By contributing to all three observed subcomplexes, the EP400 subunit serves as a scaffold that connects and coordinates them into one supercomplex (Fig. 3a). The huge 400-kDa EP400 subunit is a uniquely elongated, extended and spread-out protein. The N-terminal part of EP400 is not resolved in our map but was shown to bind to the highly flexible TINTIN module that includes several 'readers' of histone marks[19]. The first residues of EP400 that are observed in our map form a short α-helix that, together with another short helix donated by the DMAP1 subunit, constitutes the dwindled neck of NuA4L (Fig. 3b). The helix is followed by a loop and then a 90-residue-long HSA helix (residues 810–900) that emanates from the back of NuA4L, binds to the actin and the ACTL6A subunits to form the actin module, traverses the gap between the NuA4L and SWR1L parts and continues deep into the SWR1 part, where it binds to a third ARP (Fig. 3c). EP400 then folds into the ATPase in a position identical to that found in the yeast SWR1 complex[8] (Fig. 3d). Following the long insertion that protrudes into the RuvBL1–RuvBL2 hexamer, EP400 completes the ATPase C-lobe. It then traverses again the gap that separates NuA4L from the ATPase as a second long helix, hereafter named the counter-helix (Fig. 3c). The counter-helix is nearly parallel to the HSA and, in its path beneath the RuvBL1–RuvBL2 hexamer, binds to one of the hexamer subunits as well as to the YL1 subunit, thus contributing to the stability of the supercomplex. EP400 is then embedded again in the NuA4L core, forming interactions with a YL1 loop (residues 210–260) and several elements of EPC1 and DMAP1 to construct a new interaction hub (Fig. 3e). Finally, EP400 extends out of NuA4L as a long loop that reaches the TRRAP subunit, where EP400 folds into the SANT domain (residues 2367–2479); this is followed by a loop and two helices (C-HLX, residues 2493–2523) that envelope the FAT (helix repeats named after FRAP, ATM and TRRAP) region of TRRAP (Fig. 3f).

In all other members of the SWR1/INO80 family of chromatin remodellers, the extended HSA helix, which houses three ARPs, forms a highly mobile module placed at the periphery of the main remodeller body and is poorly resolved in the cryo-EM maps[8,9] (Extended Data Fig. 7). This mobile module was shown in INO80 to act as a sensor for extranucleosomal DNA, mainly through interaction with the HSA helix itself, which is crucial for the activity of these remodellers and regulates their recruitment to chromatin[20]. Although the TIP60-C HSA module shares some structural principles with its counterparts in other INO80/SWR1 remodellers, it also shows some key differences (Extended Data Fig. 7b–d). In TIP60-C, this module is located at the centre of the holo-complex, and it is fixed and well resolved in our maps. Most importantly, the TIP60-C HSA is occluded all along its trajectory and probably cannot serve as a DNA sensor (Fig. 3c and Extended Data Fig. 7c,d). The TIP60-C HSA module also deviates from its counterparts in its architecture. In other remodellers, the three ARPs are placed one next to another[21], whereas in TIP60-C there is a gap of 50 Å between the second and third (isolated) ARP, so that the first two are located in NuA4L whereas the third is hosted in the SWR1L part. These differences must be reflected in how these remodellers are recruited to chromatin, and we discuss this later.

The rearranged neck acts as an interaction hub

The neck is a large region that coordinates all yeast NuA4 modules[4]. This part is completely rearranged in the human complex and bears little similarity to its yeast counterpart (Fig. 4a). The most prominent feature in the yeast neck is a bundle of four long helices donated by three intertwined subunits that serves to strongly couple the TRRAP homologue, Tra1, to the actin module at the core of NuA4 (Fig. 4d,e). In the human version, we observe a highly degenerate design of this bundle, formed by the weak interaction between two short EP400 and DMAP1 helices (Fig. 4a,b). Furthermore, whereas the rest of the yeast neck is characterized by an intricate network of unfolded threads, our structure reveals that in TIP60-C, the neck is dominated by a unique construction made of eleven β-strands, with some similarity to a β-barrel (Fig. 4c). This barrel-like module is composed of strands contributed by all three neck subunits—namely, EP400, EPC1 and DMAP1—and forms a tight interaction between these proteins. Moreover, this construction acts as a hub that coordinates not only other modules of NuA4L, but also the contact between NuA4L and SWR1L, as well as TRRAP. The hub is the structured formation immediately preceding the unfolded EPC1 loop that extends towards the KAT module, and it also contains the EP400 loop that leads to the SANT domain connecting to TRRAP. The hub further interacts with the HSA helix and the ARPs. Finally, this construction immediately succeeds the EP400 counter-helix that returns from SWR1L, embedding EP400 back into NuA4L. The fully rearranged neck domain is thus designed to interconnect NuA4L with SWR1L as well as with TRRAP, and to conserve its role in coordinating the functional TIP60-C modules.

Implications for function and mechanism

As we have shown, TIP60-C exhibits fundamental structural differences with respect to its individual yeast counterparts. A completely altered neck architecture and a mobile docking platform for activators sets it apart from NuA4. A static actin module placed close to the

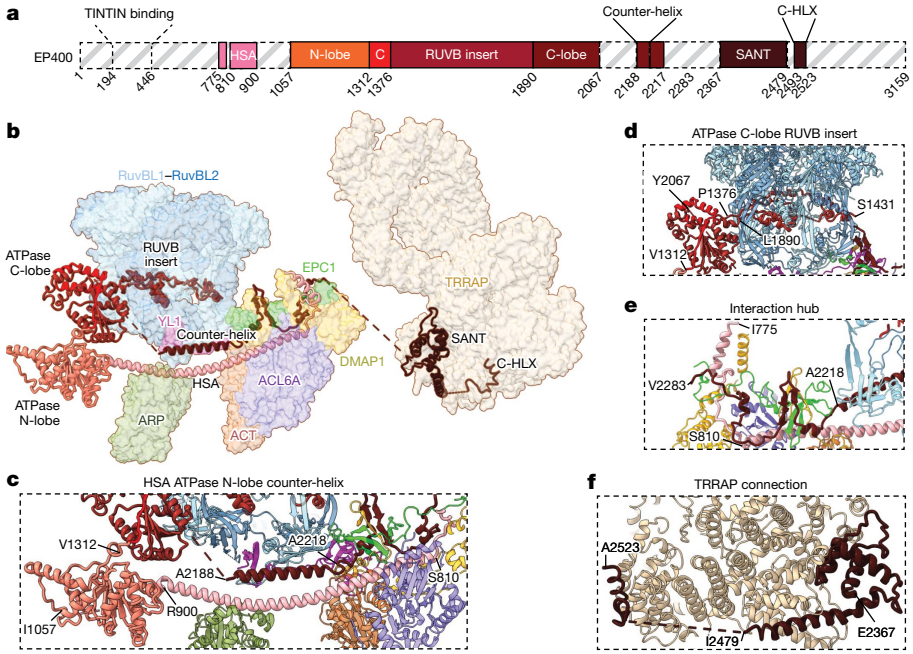

Fig. 3 | EP400 scaffolds the three TIP60-C lobes. **a**, Domain organization of EP400. The domain boundaries are marked with residue numbers, and the coloured parts correspond to the modelled domains. C-HLX, α-helix C-terminal of the SANT domain. **b**, Representation of the EP400 domains within TIP60-C. Colours of EP400 domains as in **a**. **c**–**f**, Enlarged views of key EP400 domains (**c**, HSA, ATPase N-lobe and counter-helix; **d**, ATPase C-lobe RUVB insert; **e**, interaction hub; and **f**, TRRAP connection) and their interactions with TIP60-C subunits.

core and pointing towards the EP400 ATPase, an occluded HSA with a specific spread of actins along the helix, as well as the absence of the Swc6–Arp6 dimer, distinguish it from SWR1. To gain insight into how these differences and the unique connections between the parts of the supercomplex might affect the TIP60-C mechanism, we first modelled a nucleosome into the SWR1L part of TIP60-C, guided by the structure of yeast SWR1–nucleosome[8] (Fig. 5a). The modelled nucleosome is clasped between the ATPase, the last turns of the HSA helix and the third, isolated, ARP that is carried by the HSA (mass-spectrometry data suggest that it is an additional copy of either ACTL6 or actin). We therefore believe that the tip of the HSA helix, and possibly the third ARP, have the role of a grip, analogous to a remodeller with a mechanical motor[20]. Sequence alignment shows that the tip of the HSA, also known as the post-HSA, is the most conserved part of this helix among all remodellers, thus suggesting a common function (Extended Data Fig. 7a). It was proposed in the INO80 and SWR1 remodellers that the grip maintains the DNA and octamer in place as the ATPase motor pumps DNA into the nucleosome, yielding a gradually growing strain in the DNA and

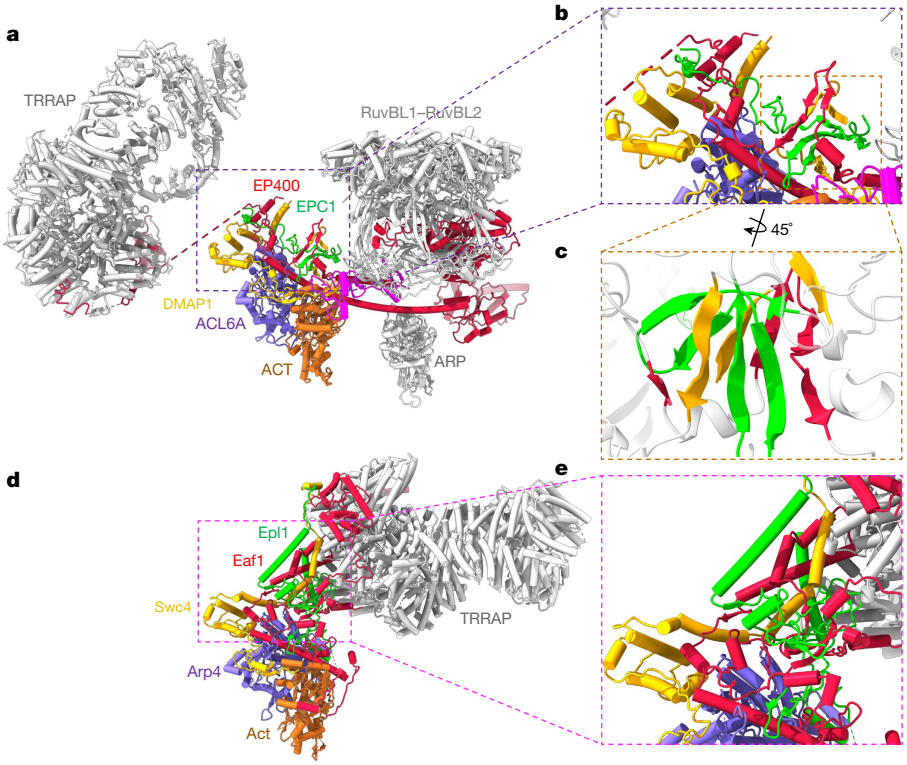

Fig. 4 | Comparison between TIP60-C and NuA4. **a**, Side view of TIP60-C showing in colour the NuA4L lobe and the scaffolding EP400 subunit. **b**, Enlarged view of the neck domain of human TIP60-C boxed in **a**. **c**, View of the β-barrel interaction hub highlighted by dotted lines in **b**, and rotated by 45°. **d**, View of yeast NuA4 in which the actin module is aligned on the ACL6A–ACT module of NuA4L. **e**, Enlarged view of the neck domain of yeast NuA4 boxed in **d**.

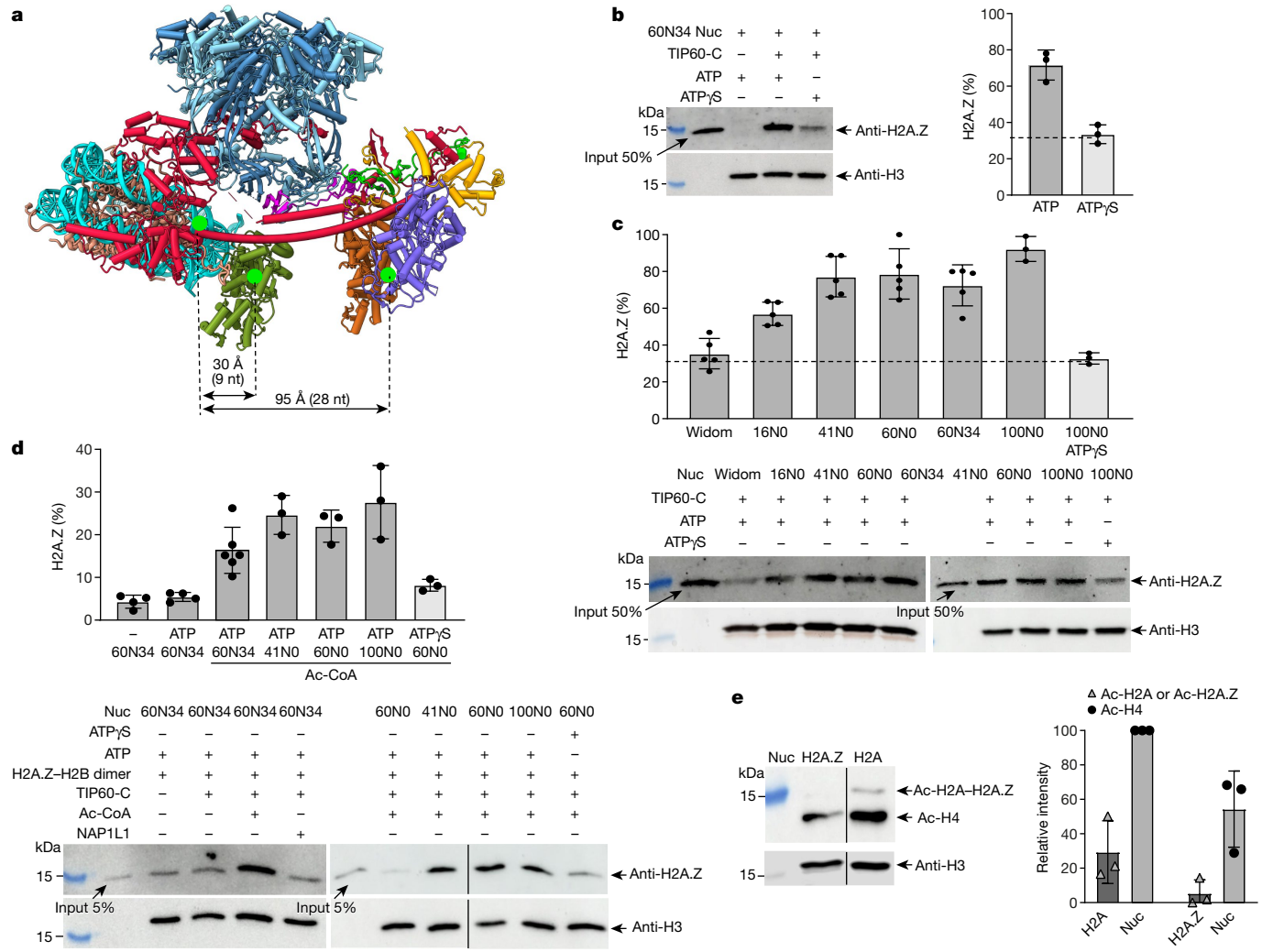

Fig. 5 | Function of TIP60-C. a, Nucleosome modelled into TIP60-C according to the yeast SWR1 structure[8]. Distances, and their approximate equivalent lengths of linear DNA base pairs, from the exit site of DNA to the ARP subunits are marked. **b**, Incorporation of endogenous TIP60-C-bound H2A.Z–H2B into 60N34 nucleosomes (Nuc) in an ATP-dependent manner. H2A.Z incorporated into the nucleosome and H3 (control) are detected by western blots. Bars represent the proportion of H2A.Z incorporated out of the total H2A.Z bound to purified TIP60-C. **c**, The efficiency of H2A.Z incorporation increases with DNA linker length until 40 bp. 'Widom' denotes 147-bp nucleosome core particles, and '*x*N*y*' denotes nucleosomes with linker lengths *x* and *y*. Dotted line indicates background levels of H2A.Z deposition. **d**, Incorporation of exogenous H2A.Z–H2B present in excess is stimulated by acetyl-CoA and is not enhanced by nucleosome DNA linker longer than 41 bp. Bars represent the proportion of H2A.Z incorporated into nucleosome out of the total H2A.Z present in the reaction. NAP1L1 is a histone chaperone. **e**, TIP60-C acetylation of nucleosomes with either H2A or H2A.Z. Acetylation was detected by an antibody for acetyl-lysine. Graphs in **b**–**e** represent the average measurement of three independent replicates (bars) with s.d. (error bars). Vertical lines in **d**,**e** represent the position where the original blots have been spliced.

causing a disruption of DNA–histone contacts that could drive histone exchange[21]. In the INO80 and SWR1 remodellers, the grip and ATPase are located at opposite sides of the nucleosome disc, and are thus separated by a long stretch of DNA (Extended Data Fig. 7b). By contrast, the grip and motor are separated by less than one DNA turn in TIP60-C, allowing the development of considerable strain in the DNA with fewer ATPase strokes. Furthermore, unlike INO80 or SWR1, the TIP60-C grip is able to bind to two DNA segments as the HSA tip contacts nucleosomal DNA close to its dyad, and the third ARP associates with the DNA linker (Fig. 5a). Notably, this position of the third ARP is similar to that of the linker histone H1 in the chromatosome[22]. We suggest that disruptions of DNA–histone contacts are accumulated and propagated differently in TIP60-C, perhaps reflecting its wider range of activities, which also include the incorporation of the H3.3 histone variant.

Other domains of TIP60-C that possibly bind to the nucleosome DNA linker include the NuA4L actin module, which might contact DNA located 95 Å or around 30 bp from the nucleosome core (Fig. 5a). To lend support to our placement of the nucleosome, we compared the H2A.Z deposition activity of TIP60-C on nucleosomes with varied DNA-linker length. We first show that endogenously TIP60-C-bound H2A.Z is incorporated into nucleosomes with two long linkers in an ATP-dependent manner (Fig. 5b). By contrast, nucleosomes with no linker (Widom) yielded a H2A.Z deposition activity that was only slightly higher than background (Fig. 5c). A short 16-bp linker (16N0) already increased the activity significantly, in line with our model, in which such a linker would form considerable interactions with the third ARP. Of note, it has been shown that the conserved actin core of ARPs can indeed bind to DNA[9]. Increasing the linker length to 41 bp (41N0) resulted in a further substantial increase of exchange efficiency, supporting the likelihood of additional DNA interactions with the NuA4L actin module. The YL1 homologue Swc2 has been shown to sense extranucleosomal DNA in yeast SWR1 (refs. 23,24). We cannot therefore exclude the possibility that the increased activity is partially due to enhanced YL1–DNA interactions, but it seems that Swc2 is mainly implicated in binding longer free

DNA. Also, consistent with the third ARP binding to only one of the DNA linkers, addition of a second linker (60N34) did not enhance activity.

Crucially, a linker longer than 41 bp (Fig. 5c,d) increased the remodelling activity only very moderately (60N0, 100N0). This is in sharp contrast to SWR1, in which a marked increase in activity is observed when the linker DNA exceeds 40 bp (ref. 23), and to INO80, in which only a long linker allows the flexible actin module to bind to extranucleosomal DNA and allosterically regulate the ATPase motor[21]. This points to fundamental differences between TIP60-C, INO80 and SWR1 in their mode of recruitment to chromatin and their regulation. SWR1 and its direct human homologue SRCAP, which lacks a NuA4L part, are thought to be enlisted to chromatin through their high affinity to the long stretches of free DNA (more than 40 bp) that occur at gene promoters[23,24]. In INO80, and possibly SWR1, the mobile actin module senses such long stretches to couple the ATPase motor to productive cycles[20,21,25]. Our biochemical tests—which did not find any increase in activity with long DNA—as well as the static actin module and the position of the obstructed HSA helix show that this is not the case for TIP60-C. Instead, the supercomplex probably uses the TRRAP docking platform of transcription activators for recruitment to specific DNA sites. TRRAP, or its yeast homologue Tra1, serve this role in NuA4 and SAGA. However, in these complexes, TRRAP is firmly bound to their cores, and flexibility is endowed to their enzymatic modules[4,26]. A highly dynamic TRRAP is probably necessary in TIP60-C to allow the relatively rigid and fixed SWR1L part to search for a suitable target. Furthermore, we observe much higher H2A.Z exchange activity when acetyl-CoA is present in the reaction mixture (Fig. 5d). This suggests that acetylation of H2A and H4 on the nucleosome by TIP60-C itself stimulates exchange, in accordance with previous findings in *Drosophila* and yeast[27,28]. We suggest therefore the following order of events: TIP60-C is first recruited to chromatin by activators binding to TRRAP; nucleosomes at long range around the site of recruitment are acetylated on H2A and H4, as was observed[4,29] for yeast NuA4; and TIP60-C recognizes acetylated nucleosomes through its BRD8 or YEATS4 subunits and exchanges H2A for H2A.Z. Notably, we find that TIP60-C acetylates nucleosomes that already bear H2A.Z much less efficiently, thus preserving its acetylation potential for nucleosomes that could undergo H2A to H2A.Z exchange (Fig. 5e).

SRCAP and TIP60-C are therefore wired to target different sites on chromatin. Indeed, there is little overlap between the in vivo activities of the complexes, because mutations in one cannot be compensated by the other[30]. We speculate that the contradictory roles of H2A.Z in promoters can be traced, at least in part, to the different machinery that was used to deposit it. Indeed, H2A.Z exchange by TIP60-C entails further acetylation of histones, as well as non-histone targets and the recruitment of additional factors, possibly leading to a different outcome as compared with exchange performed by SRCAP. Merging exchange and acetylation seems to be linked to cell-fate decisions and differentiation. In certain circumstances, SWR1 and NuA4 are joined even in unicellular organisms; for example, in polymorphic *Candida albicans* strains during the reversible yeast–hyphae transition[31]. Although TIP60-C is essential for embryonic development in mice[32], conditional knockout of *Tip60* in differentiated liver cells has only moderate effects[33].

Online content

Any methods, additional references, Nature Portfolio reporting summaries, source data, extended data, supplementary information, acknowledgements, peer review information; details of author contributions and competing interests; and statements of data and code availability are available at https://doi.org/10.1038/s41586-024-08011-w.

1. Bannister, A. J. & Kouzarides, T. Regulation of chromatin by histone modifications. *Cell Res.* **21**, 381–395 (2011).
2. Auger, A. et al. Eaf1 is the platform for NuA4 molecular assembly that evolutionarily links chromatin acetylation to ATP-dependent exchange of histone H2A variants. *Mol. Cell. Biol.* **28**, 2257–2270 (2008).
3. Jacquet, K. et al. The TIP60 complex regulates bivalent chromatin recognition by 53BP1 through direct H4K20me binding and H2AK15 acetylation. *Mol. Cell* **62**, 409–421 (2016).
4. Frechard, A. et al. The structure of the NuA4–Tip60 complex reveals the mechanism and importance of long-range chromatin modification. *Nat. Struct. Mol. Biol.* **30**, 1337–1345 (2023).
5. Qu, K., Chen, K., Wang, H., Li, X. & Chen, Z. Structure of the NuA4 acetyltransferase complex bound to the nucleosome. *Nature* **610**, 569–574 (2022).
6. Zukin, S. A. et al. Structure and flexibility of the yeast NuA4 histone acetyltransferase complex. *eLife* **11**, e81400 (2022).
7. Ji, L. et al. Structure of the NuA4 histone acetyltransferase complex. *Proc. Natl Acad. Sci. USA* **119**, e2214313119 (2022).
8. Willhoft, O. et al. Structure and dynamics of the yeast SWR1–nucleosome complex. *Science* **362**, eaat7716 (2018).
9. Eustermann, S. et al. Structural basis for ATP-dependent chromatin remodelling by the INO80 complex. *Nature* **556**, 386–390 (2018).
10. Biterge, B. & Schneider, R. Histone variants: key players of chromatin. *Cell Tissue Res.* **356**, 457–466 (2014).
11. Cai, Y. et al. Identification of new subunits of the multiprotein mammalian TRRAP/TIP60-containing histone acetyltransferase complex. *J. Biol. Chem.* **278**, 42733–42736 (2003).
12. Allis, C. D. & Jenuwein, T. The molecular hallmarks of epigenetic control. *Nat. Rev. Genet.* **17**, 487–500 (2016).
13. Lashgari, A., Kougnassoukou Tchara, P. E., Lambert, J. P. & Cote, J. New insights into the DNA repair pathway choice with NuA4/TIP60. *DNA Repair* **113**, 103315 (2022).
14. Giaimo, B. D., Ferrante, F., Herchenrother, A., Hake, S. B. & Borggrefe, T. The histone variant H2A.Z in gene regulation. *Epigenetics Chromatin* **12**, 37 (2019).
15. Kreienbaum, C., Paasche, L. W. & Hake, S. B. H2A.Z's 'social' network: functional partners of an enigmatic histone variant. *Trends Biochem. Sci.* **47**, 909–920 (2022).
16. Martin, B. J. E. et al. Global identification of SWI/SNF targets reveals compensation by EP400.*Cell* **186**, 5290–5307 (2023).
17. Park, J. H., Sun, X. J. & Roeder, R. G. The SANT domain of p400 ATPase represses acetyltransferase activity and coactivator function of TIP60 in basal p21 gene expression. *Mol. Cell. Biol.* **30**, 2750–2761 (2010).
18. Brown, C. E. et al. Recruitment of HAT complexes by direct activator interactions with the ATM-related Tra1 subunit. *Science* **292**, 2333–2337 (2001).
19. Devoucoux, M. et al. MRG proteins are shared by multiple protein complexes with distinct functions. *Mol. Cell. Proteomics* **21**, 100253 (2022).
20. Jungblut, A., Hopfner, K. P. & Eustermann, S. Megadalton chromatin remodelers: common principles for versatile functions. *Curr. Opin. Struct. Biol.* **64**, 134–144 (2020).
21. Kunert, F. et al. Structural mechanism of extranucleosomal DNA readout by the INO80 complex. *Sci. Adv.* **8**, eadd3189 (2022).
22. Dombrowski, M., Engeholm, M., Dienemann, C., Dodonova, S. & Cramer, P. Histone H1 binding to nucleosome arrays depends on linker DNA length and trajectory. *Nat. Struct. Mol. Biol.* **29**, 493–501 (2022).
23. Ranjan, A. et al. Nucleosome-free region dominates histone acetylation in targeting SWR1 to promoters for H2A.Z replacement. *Cell* **154**, 1232–1245 (2013).
24. Yen, K., Vinayachandran, V. & Pugh, B. F. SWR-C and INO80 chromatin remodelers recognize nucleosome-free regions near +1 nucleosomes. *Cell* **154**, 1246–1256 (2013).
25. Oberbeckmann, E. et al. Ruler elements in chromatin remodelers set nucleosome array spacing and phasing. *Nat. Commun.* **12**, 3232 (2021).
26. Papai, G. et al. Structure of SAGA and mechanism of TBP deposition on gene promoters. *Nature* **577**, 711–716 (2020).
27. Kusch, T. et al. Acetylation by Tip60 is required for selective histone variant exchange at DNA lesions. *Science* **306**, 2084–2087 (2004).
28. Altaf, M. et al. NuA4-dependent acetylation of nucleosomal histones H4 and H2A directly stimulates incorporation of H2A.Z by the SWR1 complex. *J. Biol. Chem.* **285**, 15966–15977 (2010).
29. Vignali, M., Steger, D. J., Neely, K. E. & Workman, J. L. Distribution of acetylated histones resulting from Gal4–VP16 recruitment of SAGA and NuA4 complexes. *EMBO J.* **19**, 2629–2640 (2000).
30. Berta, D. G. et al. Deficient H2A.Z deposition is associated with genesis of uterine leiomyoma. *Nature* **596**, 398–403 (2021).
31. Wang, X. et al. Merge and separation of NuA4 and SWR1 complexes control cell fate plasticity in *Candida albicans*. *Cell Discov.* **4**, 45 (2018).
32. Hu, Y. et al. Homozygous disruption of the *tip60* gene causes early embryonic lethality. *Dev. Dyn.* **238**, 2912–2921 (2009).
33. Kocpinar, E. F., Baltaci, N. G., Akkemik, E. & Budak, H. Depletion of *Tip60*/*Kat5* affects the hepatic antioxidant system in mice. *J. Cell. Biochem.* **124**, 103–117 (2023).

Methods

Establishment of the K562 cell line with a SBP-3×Flag-tagged EPC1

To create a K562 EPC1-SBP-3×Flag cell line, 2×10^6 K562 cells (obtained from ATCC) were transfected by electroporation (Amaxa2D, program X001; Lonza solution V) with 2 μg of pX458 plasmid expressing Cas9, eGFP and guide RNA against the *EPC1* locus (targeting DNA cleavage immediately 3′ to the *EPC1* STOP codon), and 9 μg of EPC1-SBP-3×Flag donor plasmid. Directly after, transfected cells were treated with 2 μM M3814 (Selleckchem), a DNA-PK inhibitor[34]. Three days after transfection, GFP-positive cells were sorted (BD FACS sorter Melody) and single-cell-derived clones were screened by PCR and Sanger sequencing for precise integration of the SBP-3×Flag tag at the *EPC1* locus. Expression of EPC1-SBP-3×Flag was confirmed by western blot using anti-Flag antibody (M2, Sigma Aldrich) and one of the K562 EPC1-SBP-3×Flag clones, named K562 EPC1-SBP-3×Flag #1D1, was expanded for purification of TIP60-C.

Purification of TIP60-C

The K562 cell line, in which the endogenous subunit EPC1 was fused at the C terminus to an SBP-3×Flag affinity tag, was cultured in PRMI medium supplemented with 10% calf serum and 50 μg ml^{-1} gentamycin. All of the following steps were performed at 0–4 °C. Six-litre cultures were centrifuged (1,000*g* for 10 min). Nuclear extraction then followed a previously published protocol[35] with several modifications. Cell pellets were first washed in cold phosphate-buffered saline (PBS) and then in buffer K75 (10 mM HEPES, pH 7.9, 75 mM KCl, 1.5 mM $MgCl_2$, 1 mM DTT, 0.5 mM PMSF, 5 μg ml^{-1} pepstaine A and 3 μg ml^{-1} E64). Cell pellets were resuspended in hypotonic K0 buffer (10 mM HEPES, pH 7.9, 1.5 mM $MgCl_2$, 1 mM DTT, 0.5 mM PMSF, 5 μg ml^{-1} pepstaine A, 3 μg ml^{-1} E64 and ROCHE protease inhibitor cocktail) and homogenized in a 100-ml Dounce homogenizer. Sucrose was added (final 10% w/v) and nuclei were pelleted for 25 min at 5,000*g*. Nuclear pellet was washed once with sucrose buffer (10 mM HEPES, pH 7.9, 1.5 mM $MgCl_2$, 10 mM KCl, 1 mM DTT, 0.5 mM PMSF, 5 μg ml^{-1} pepstaine A, 3 μg ml^{-1} E64 and 10% sucrose w/v). Nuclear pellets were resuspended in no-salt buffer (20 mM HEPES, pH 7.9, 25% glycerol, 1.5 mM $MgCl_2$, 2 mM DTT, 0.5 mM PMSF, 5 μg ml^{-1} pepstaine A, 3 μg ml^{-1} E64 and ROCHE protease inhibitor cocktail) and homogenized in a 40-ml Dounce homogenizer. NaCl was added to a final concentration of 0.3 M before a 30-min incubation with rotation. The nuclear extract was cleared by centrifugation (30,000*g* for 30 min) and frozen in liquid nitrogen. Low concentrations of PEG 20,000 as well as 5 mM $MgCl_2$ were added to precipitate some remaining organelles and membrane parts by a short centrifugation (33,000*g* for 10 min). The PEG 20,000 concentration was then increased to 5–6% and TIP60-C was precipitated in a second short centrifugation step. The pellet was resuspended in a minimal volume and was incubated with anti-flag M2 agarose beads overnight in buffer A (20 mM HEPES pH 8.0, 250 mM sodium chloride, 10% sucrose, 2 mM $MgCl_2$, 0.5 mM DTT, 0.5 mM PMSF, 5 μg ml^{-1} pepstaine A and 3 μg ml^{-1} E64). The beads were washed four times with buffer A supplemented with 0.05% Tween-20 and finally eluted with buffer A containing 150 μg ml^{-1} 3×Flag peptide. The eluate was either directly used for histone exchange assays or further purified for cryo-EM. Elution from the Flag beads was mixed with streptavidin beads and incubated for four hours. The beads were washed three times with buffer B (20 mM HEPES pH 8.0, 250 mM sodium chloride, 10% sucrose, 2 mM $MgCl_2$, 1 mM DTT and 0.05% Tween-20) and finally eluted with either buffer C (20 mM HEPES pH 8.0, 250 mM sodium chloride, 10% sucrose, 2 mM $MgCl_2$, 1 mM DTT, 20 mM biotin and 0.05% Tween-20) for the in vitro acetylation activity test, or buffer D (20 mM HEPES pH 8.0, 250 mM sodium chloride, 1% trehalose, 2 mM $MgCl_2$, 1 mM DTT, 20 mM biotin and 0.0025% dodecyl-maltoside) for cryo-EM analysis. TIP60-C was flash-frozen in liquid nitrogen and stored at −80 °C.

Reconstitution of histone octamers and preparation of nucleosome DNA

Octamers were reconstituted from individual *Xenopus laevis* (canonical) or human (H2A.Z) histones expressed as inclusion bodies according to the standard protocol[36,37].

The biotinylated nucleosomal DNAs Widom, 16N0, 41N0, 60N0, 60N34 and 100N0 were generated by PCR (‘*x*Ny’ corresponds to nucleosomes with linker lengths *x* and *y*). In-house purified Phusion polymerase was used for the PCR reaction on the following template:

CGACGGCCAGTGAACCACGATTCGGTACTCGGGTTCTAGACCATGA
TTACGCCAAGCTTTCCTATGACTCATCCAGTTCTGCAGGCGATCACT
ACATGC**ACAGGATGGCTAGCTCTGACACGTGCCTGGAGACTAGGGA
GTAATCCCCTTGGCGGTTAAAACGCGGGGGACAGCGCGTACGTGC
GTTTAAGCGGTGCTAGAGCTGTCTACGACCAATTGAGCGGCCTCGG
CACCGGGATTCTCGCA**TCTAACTCCCGGGTGTGCCTATAAAAGGAT

(The Widom-601 positioning sequence is in bold and the PstI restriction site is underlined). The primers used for the PCR reactions were: biotin–GGCGATCACTACATGCACAGGATGGCTAGC for the 16-bp linker, biotin–AGCCGGAGGACAGTCCTCCGCTGCAGGCGATCACTACATGCAC AGGATG for the 41-bp linker, biotin–GATTACGCCAAGCTTAGCCGG AGGACAGTCCTCCGCTGCAGGCGATCACTACATGCACAGGATG for the 60-bp linker, biotin–CGACGGCCAGTGAACCACGATTCGG for the 100-bp linker, TGCGAGAATCCCGGTGCCGAGGCCG for the 0-bp linker reverse primer and ATCCTTTTATAGGCACACCCGGGAGTTAGATGCG for the 34-bp linker reverse primer. The PCR products were purified on Macherey-Nagel nucleospin plasmid columns (ref. 740588.50; 1 column per 0.5 ml PCR mixture) using solutions from Macherey-Nagel Gel and PCR Clean-up kit (ref. 740609.50) according to PCR clean-up protocol. The eluted DNA was precipitated with 0.3 M sodium acetate and 70% ethanol. DNA pellet was dissolved in 1× TE buffer (10 mM Tris-HCl pH 7.5, 1 mM EDTA).

Reconstitution of nucleosomes

Nucleosomes with a 147-bp Widom-601 positioning sequence with linkers of different length were prepared according to the NEB Dilution Assembly Protocol (E5350) (https://international.neb.com/protocols/2012/06/02/dilution-assembly-protocol-e5350) with the following modifications: 2.75 μM DNA was mixed with 2.75 μM canonical or H2A.Z histone octamers in a solution containing 2 M NaCl, 1 mM EDTA and 5 mM β-mercaptoethanol. The solution was incubated for 30 min at room temperature and then underwent serial dilutions down to 1.48 M, 1 M, 0.6 M and 0.25 M NaCl with low-salt buffer (10 mM HEPES-KOH pH 8.0 and 2.5 mM β-mercaptoethanol). After each dilution, the solution was incubated at room temperature for 30 min. To reduce the final NaCl concentration, nucleosomes were concentrated in 0.5-ml 100-kDa cut-off Amicon Ultra filter up to 100 μl, then diluted five times with low-salt buffer. This step was repeated one more time. Finally, nucleosomes were concentrated to 3–4 μM and analysed in a 5% native 0.2× TBE polyacrylamide gel to ascertain the quality of the sample and the absence of free DNA.

Reconstitution of the H2A.Z–H2B dimer

Two milligrams of lyophilized monomers of H2A.Z and H2B were dissolved in 7 M guanidine hydrochloride, 20 mM Tris pH 7.5 and 10 mM DTT at room temperature, and mixed in stoichiometric amounts. The mixture was dialysed against three changes of refolding buffer (10 mM Tris pH 7.5, 2 M NaCl, 1 mM EDTA and 7 mM β-mercaptoethanol), and H2A.Z–H2B dimer was purified over a Superdex 200 column (GE Healthcare) pre-equilibrated with GF buffer (20 mM Tris pH 7.5, 2 M NaCl, 1 mM EDTA and 0.5 mM TCEP). Glycerol was added (final concentration 20% w/v) to H2A.Z–H2B dimers, which were then aliquoted, flash-frozen in liquid nitrogen and stored at −80 °C.

Histone acetyltransferase assay

Reactions were performed in 20 mM HEPES (pH 7.5), 50 mM NaCl, 50 µM acetyl-CoA, 0.1 mg ml^{-1} BSA, 2 mM $MgCl_2$, 0.2 mM TCEP, 1 µM $ZnSO_4$, 5 µM trichostatin A, 10% (v/v) glycerol and 1 µM nucleosome. The reactions were initiated by adding 10 nM TIP60-C. After an incubation at 30 °C for 30 min, the reactions were stopped by adding SDS loading buffer and heating at 95 °C for 3 min. Proteins were then resolved by 15% SDS–PAGE and analysed by western blot, applying a primary antibody against acetylated lysine (Cell Signaling Technology, 9441S). The levels of histone H3 revealed by primary antibodies (Cell Signaling Technology, 14269) were used as a control.

Histone exchange assay

To test whether the TIP60-C-bound H2A.Z–H2B (that is, endogenous histones that are part of the purified complex) can be incorporated by TIP60-C into nucleosomes, 200 nM of biotinylated mono-nucleosomes with the indicated DNA linker length were mixed with 20 nM TIP60-C in 20 µl histone exchange buffer (20 mM HEPES, pH 7.5, 50 mM NaCl, 5 mM $MgCL_2$, 10% glycerol, 0.1 mg ml^{-1} BSA, 1 mM ATP or ATPγS and 0.05% Tween-20), and incubated at 30 °C for 2 h. Ionic strength was increased by the addition of 0.6 µl 5 M NaCl to prevent non-specific association of TIP60-C with beads and the reaction mix was then incubated (6 °C, 30 min, 1,250 rpm shaking in ThermoMixer C) with 6 µl streptavidin magnetic beads (Thermo Fisher Scientific, 88816) pre-equilibrated with washing buffer (20 mM HEPES, pH 7.5, 250 mM NaCl, 5 mM $MgCl_2$, 10% glycerol, 0.1 mg ml^{-1} BSA and 0.05% Tween-20). Beads were then pelleted and resuspended in 50 µl washing buffer with 2 mM ATPγS for 5 min at room temperature to further eliminate any non-specific association of TIP60-C. After three times of washing as above, 10 µl of 1× SDS loading buffer was added and heated at 95 °C for 3 min. Proteins were then resolved by 15% SDS–PAGE that was followed by a western blot with a primary antibody against H2A.Z (Cell Signaling Technology, 2718). Western blot using primary antibody against H3 (Cell Signaling Technology, 14269) was done as control.

When testing H2A.Z exchange by TIP60-C in the presence of excess H2A.Z–H2B dimers, we encountered the difficulty presented by high-background due to non-specific binding of H2A.Z to nucleosome linker DNA as well as to salmon sperm DNA that associates with the beads[28]. To overcome this issue, we took advantage of a PstI site located on the long DNA linker close to the nucleosome core. Cutting with the restriction enzyme released the core nucleosome from the beads, carrying with it only traces of non-specifically bound H2A.Z. For each reaction, 200 nM of biotinylated mono-nucleosomes were mixed with 20 nM TIP60-C and 400 nM H2A.Z–H2B dimer in 20 µl histone exchange buffer (20 mM HEPES, pH 7.5, 50 mM NaCl, 5 mM $MgCL_2$, 10% glycerol, 0.1 mg ml^{-1} BSA, 1 mM ATP and 0.05% Tween-20, with or without 50 µM acetyl-CoA), and incubated at 30 °C for 2 h. Two microlitres of quenching solution (4 mg ml^{-1} salmon sperm DNA, 100 mM EDTA and 10 mM ATPγS) was added, and incubated at 37 °C for 30 min. The reaction mixture was then incubated with 6 µl streptavidin magnetic beads for 30 min at 6 °C. Beads were pelleted and then resuspended in 50 µl washing buffer for 5 min at room temperature. After three washes, 20 µl of restriction enzyme solution (20 mM HEPES, pH 7.5, 50 mM NaCl, 5 mM $MgCl_2$, 10% glycerol, 0.1 mg ml^{-1} BSA, 0.05% Tween-20 and 20 U PstI-HF) was added, and incubated at 37 °C for 1 h at 1,250 rpm in a ThermoMixer C (Eppendorf). The supernatant containing the released nucleosomes was collected, mixed with SDS loading buffer and heated at 95 °C for 3 min. The results were analysed by western blot as above. Quantification of signal intensity was performed on digitally acquired images (ImageQuant 800, Cytiva Life Sciences) by ImageJ. All statistical tests were performed using Prism.

Cryo-EM sample preparation and data acquisition

Three microlitres of sample was applied onto a holey gold grid (UltrAuFoil R1.2/1.3 300 mesh) rendered hydrophilic by a 90-s treatment in a Fischione 1070 plasma cleaner operating at 34% power with a gas mixture of 80% argon:20% oxygen. The grid was blotted for 1.5 s at blot force 8 and flash-frozen in liquid ethane using a Vitrobot Mark IV (FEI) at 4 °C and 95–100% humidity. Two different datasets were collected. The first dataset was acquired on a Cs-corrected Titan Krios (Thermo Fisher Scientific) microscope operating at 300 kV in nanoprobe mode using serialEM for automated data collection[38]. Movie frames were recorded on a Gatan K3 direct electron detector after a Quantum LS 967 energy filter using a 20-eV slit width in zero-loss mode. Images were acquired hardware-binned at a nominal magnification of 81,000×, which yielded a pixel size of 0.862 Å. Forty movie frames were recorded at a dose of 1.12 and 1.30 e^- per $Å^2$ per frame. To improve resolution on the SWR1L and NuA4L parts, a second image dataset was acquired on a Titan Krios G4 microscope operating at 300 kV in nanoprobe mode using SerialEM for automated data collection. Movie frames were recorded on a Falcon 4i direct electron detector after a Selectris X energy filter using a 10-eV slit width in zero-loss mode. Images were acquired at a nominal magnification of 165,000×, which yielded a pixel size of 0.73 Å.

Image processing

For the first dataset, WARP was used to perform the initial pre-processing steps, align movie frames, perform dose-weighting, correct the beam-induced specimen motion and estimate the contrast transfer function (CTF)[39]. After visual inspection, images with poor CTF, showing particle aggregation or abundant ice contamination were discarded. The second dataset was pre-processed using cryoSPARC[40]. Particle coordinates were determined using crYOLO[41] for both datasets. The datasets were analysed in RELION-3.1 (ref. 42) and cryoSPARC according to standard protocols. In brief, three rounds of reference-free two-dimensional (2D) classification of the individual particle images were performed in cryoSPARC to remove images corresponding to contaminating or damaged particles and ice contaminations. References (3D models) were generated by the ab initio 3D reconstruction program of cryoSPARC. These structures were then used as references for 3D classification jobs in cryoSPARC and particles corresponding to high-resolution 3D classes were selected and used for non-uniform refinement. Refined particles were subjected to 3D classification in RELION without alignment using various regularization parameter (T) values. Particles corresponding to high-resolution classes were used in the subsequent non-uniform refinement in cryoSPARC. We performed a focused refinement of different parts of TIP60-C as follows. Particles were binned to a pixel size of 2 Å and were subjected to 3D classifications in RELION using masks. After visual inspection, particles corresponding to the best classes were refined in cryoSPARC locally with a mask covering the region of interest. Global resolution estimates were determined using the Fourier shell correlation (FSC) = 0.143 criterion after a gold-standard refinement. Local resolutions were estimated with cryoSPARC. To analyse the heterogeneity in the cryo-EM map owing to the presence of the flexible TRRAP module (430 kDa), we used the neural-network-based cryoDRGN[43] and OPUS-DSD[44] reconstruction to map the particles on two principal components. We partitioned the latent space into 20 regions and a density map was generated from the centre of each region.

Model building

RuvBL1–RuvBL2 hexamer was extracted from the human INO80–nucleosome structure (Protein Data Bank (PDB) 6HTS), placed into the map by rigid body fitting in Chimera[45] and used as a starting point for manual editing in Coot[46]. The EP400 ATPase C-lobe was modelled in AlphaFold[47], docked into the map by ADP_EM[48] and manually adjusted according to density. The EP400 insertion into the hexamer was then manually built. This was facilitated by secondary structure prediction in RaptorX[49]. The ATPase N-lobe was modelled in AlphaFold and docked by ADP_EM into the map generated by focused refinement of this region in SWR1L. An actin molecule was docked into the same

map as the third ARP. Mass spectrometry suggests that this protein is an additional copy of either actin or ACTL6A. The TRRAP structure was extracted from PDB 7KTR and fitted into the corresponding map. Manual adjustment of TRRAP and building of some additional loops, where density was clearly visible, were carried out. The structure of yeast NuA4 (PDB 7ZVW) served as a starting point for building the actin module. The rest of the NuA4L core and the novel interaction hub were manually built into a map generated by focused refinement on NuA4L. Manual model building was guided by secondary structure prediction and the density of bulky side chains (Lys, His, Arg, Phe, Tyr and Trp). The YL1– VPS71 subunit was also manually built, as were the HSA helix and the counter-helix. The atomic model was refined in PHENIX by real-space refinement with secondary structure restrains[50] and in Isolde[51]. All display images were generated using ChimeraX[52].

Reporting summary

Further information on research design is available in the Nature Portfolio Reporting Summary linked to this article.

Data availability

The experimental cryo-EM maps have been deposited in the Electron Microscopy Data Bank (EMBD) under accession codes EMD-18581, EMD-18591, EMD-18597, EMD-18598, EMD-18612, EMD-18613, EMD-18618 and EMD-18794. Two composite maps were also deposited for TIP60-C (EMDB-18611) and the TRRAP module (EMDB-18619). The model coordinates for the TIP60-C core and the TRRAP module derived from the composite maps have been deposited in the PDB database under the accession codes 8QR1 and 8QRI, respectively.

34. Riesenberg, S. et al. Simultaneous precise editing of multiple genes in human cells. *Nucleic Acids Res.* **47**, e116 (2019).
35. Dignam, J. D., Lebovitz, R. M. & Roeder, R. G. Accurate transcription initiation by RNA polymerase II in a soluble extract from isolated mammalian nuclei. *Nucleic Acids Res.* **11**, 1475–1489 (1983).
36. Dyer, P. N. et al. Reconstitution of nucleosome core particles from recombinant histones and DNA. *Methods Enzymol.* **375**, 23–44 (2004).
37. Luger, K., Rechsteiner, T. J. & Richmond, T. J. Expression and purification of recombinant histones and nucleosome reconstitution. *Methods Mol. Biol.* **119**, 1–16 (1999).
38. Mastronarde, D. N. Automated electron microscope tomography using robust prediction of specimen movements. *J. Struct. Biol.* **152**, 36–51 (2005).
39. Tegunov, D. & Cramer, P. Real-time cryo-electron microscopy data preprocessing with Warp. *Nat. Methods* **16**, 1146–1152 (2019).
40. Punjani, A., Rubinstein, J. L., Fleet, D. J. & Brubaker, M. A. cryoSPARC: algorithms for rapid unsupervised cryo-EM structure determination. *Nat. Methods* **14**, 290–296 (2017).
41. Wagner, T. et al. SPHIRE-crYOLO is a fast and accurate fully automated particle picker for cryo-EM. *Commun. Biol.* **2**, 218 (2019).
42. Zivanov, J. et al. New tools for automated high-resolution cryo-EM structure determination in RELION-3. *eLife* **7**, e42166 (2018).
43. Zhong, E. D., Bepler, T., Berger, B. & Davis, J. H. CryoDRGN: reconstruction of heterogeneous cryo-EM structures using neural networks. *Nat. Methods* **18**, 176–185 (2021).
44. Luo, Z., Ni, F., Wang, Q. & Ma, J. OPUS-DSD: deep structural disentanglement for cryo-EM single-particle analysis. *Nat. Methods* **20**, 1729–1738 (2023).
45. Goddard, T. D., Huang, C. C. & Ferrin, T. E. Visualizing density maps with UCSF Chimera. *J. Struct. Biol.* **157**, 281–287 (2007).
46. Emsley, P., Lohkamp, B., Scott, W. G. & Cowtan, K. Features and development of Coot. *Acta Crystallogr. D* **66**, 486–501 (2010).
47. Jumper, J. et al. Highly accurate protein structure prediction with AlphaFold. *Nature* **596**, 583–589 (2021).
48. Garzon, J. I., Kovacs, J., Abagyan, R. & Chacon, P. ADP_EM: fast exhaustive multi-resolution docking for high-throughput coverage. *Bioinformatics* **23**, 427–433 (2007).
49. Kallberg, M. et al. Template-based protein structure modeling using the RaptorX web server. *Nat. Protoc.* **7**, 1511–1522 (2012).
50. Terwilliger, T. C. Rapid model building of α-helices in electron-density maps. *Acta Crystallogr. D* **66**, 268–275 (2010).
51. Croll, T. I. ISOLDE: a physically realistic environment for model building into low-resolution electron-density maps. *Acta Crystallogr. D* **74**, 519–530 (2018).
52. Goddard, T. D. et al. UCSF ChimeraX: meeting modern challenges in visualization and analysis. *Protein Sci.* **27**, 14–25 (2018).
53. Xu, P. et al. The NuA4 core complex acetylates nucleosomal histone H4 through a double recognition mechanism. *Mol. Cell* **63**, 965–975 (2016).

Acknowledgements We thank A. Hamiche for discussions and for the gift of purified NAP1L1; the F. Zhang laboratory for pX458 (plasmid 48138 obtained from Addgene); and the mass-spectrometry service of the IGBMC for advice. We acknowledge support from the Institut National de la Santé et de la Recherche Médicale (Inserm); the Centre National pour la Recherche Scientifique (CNRS); the Ligue Contre le Cancer; the University of Strasbourg Institute for Advanced Study (USIAS) for a fellowship to P.S. (IdEx Unistra); and the Agence Nationale de la Recherche grants to P.S. (ANR-17-CE12-0022), to A.B. and J.P.C. (ANR-II-INSB-0014) and to the IGBMC (ANR-10-LABX-0030-INRT). This work of the Interdisciplinary Thematic Institute IMCBio+, as part of the ITI 2021-2028 program of the University of Strasbourg, CNRS and Inserm, was supported by IdEx Unistra (ANR-10-IDEX-0002), the SFRI-STRAT'US project (ANR-20-SFRI-0012) and EUR IMCBio (ANR-17-EURE-0023) under the framework of the France 2030 Program. We acknowledge the use of resources of the French Infrastructure for Integrated Structural Biology (FRISBI) (ANR-10-INBS-0005) and of Instruct-ERIC. The cryo-electron microscopes were co-financed by the European Regional Development Fund (ERDF), the Strasbourg Eurometropole, the Alsace Region, FRISBI and the ESR/EquipEx+ France-Cryo-EM (ANR-21-ESRE-0046).

Author contributions A.B.-S. and P.S. designed the study. J.P.C., A.B. and A.P. generated and tested the cell lines. A.B.-S., C.L. and C.S. did the TIP60-C purification. C.L., G.P. and C.C. defined conditions for grid preparation and freezing. C.L., C.C. and G.P. prepared cryo-EM samples. G.P. and C.L. collected and analysed cryo-EM data. C.L. and A.B.-S. interpreted the maps by fitting crystal coordinates and model building. C.L. and E.S. performed HAT and H2A.Z exchange activity assays. P.S. and A.B.-S. supervised the work. C.L., G.P. and P.S. prepared figures. A.B.-S., C.L. and P.S. wrote the manuscript with input from all authors.

Competing interests The authors declare no competing interests.

Additional information

Supplementary information The online version contains supplementary material available at https://doi.org/10.1038/s41586-024-08011-w.

Correspondence and requests for materials should be addressed to Adam Ben-Shem.

Peer review information *Nature* thanks Blaine Bartholomew, Alan Cheung and the other, anonymous, reviewer(s) for their contribution to the peer review of this work.

a

Sc SWR1	Sc NuA4	Hs TIP60-C	Hs SRCAP
Swr1		EP400	SRCAP
	Eaf1		
Arp4	Arp4	ACTL6A	ACTL6A
Act1	Act1	Actin	Actin
Swc4	Swc4	DMAP1	DMAP1
Yaf9	Yaf9	GAS41/YEATS4	GAS41
Swc2		YL1/VPS72	YL-1
Rvb1		RUVBL1	RUVBL1
Rvb2		RUVBL2	RUVBL2
Arp6			ARP6
Swc6			ZNHIT1
		3rd ARP	
	Tra1	TRRAP	
	Yng2	ING3	
	Epl1	EPC1	
	Esa1	TIP60	
	Eaf6	EAF6/MEAF6	
	Eaf7	MRGBP	
	Eaf3	MORF4L2/MRGX	
		MORF4L1/MRG15	
	Eaf5	BRD8	
		MBTD1	
		H2B	H2B
		H2A.Z	H2A.Z
Bdf1			
Swc3			
Swc5			
Swc7			

b

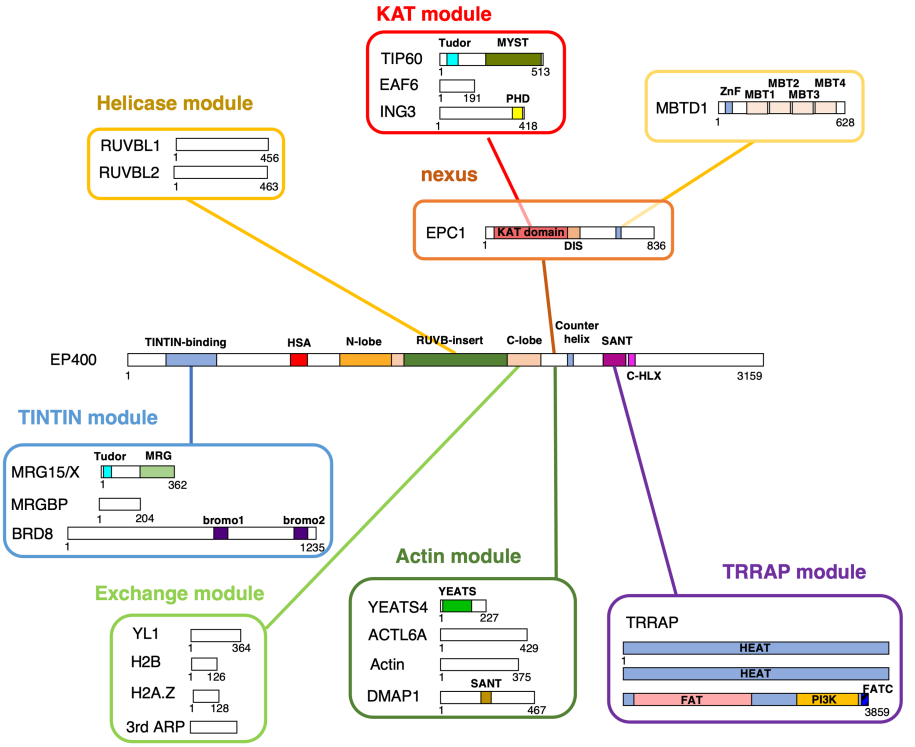

Extended Data Fig. 1 | Subunit and domain organization of the TIP60-C-related complexes. a, Subunit composition of the *Saccharomyces cerevisiae* (Sc) SWR1 and NuA4 complexes, the Human (Hs) TIP60-C and SRCAP complexes. **b**, TIP60-C subunits are organized into an enzymatic KAT module, a RUVBL1/RUVBL2 helicase module, an activator-binding TRRAP module, an actin module, a TINTIN module interconnected by a EP400 scaffolding module. Protein domains are abbreviated as follows: YEATS (Yaf9, ENL, AF9, Taf14, Sas5 domain), SANT (Swi3, Ada2, N-Cor, TFIIIB domain), DIS (disordered region), HSA (Helicase SANT associated), MYST (MOZ, Ybf2/Sas3, Sas2, Tip60 family of Histone Acetyl Transferase), PHD (plant homeodomain), HEAT (α-helical repeats found in Huntingtin, Elongation factor 3, Protein phosphatase 2A and Tor kinase), FAT (four helix bundle found in FRAP, ATM and TRRAP), FATC (kinase domain important for assembly). TINTIN (Trimer Independent of NuA4 involved in Transcription Interactions with Nucleosomes), Tudor (methyl-lysine and methyl-arginine binding domain), Znf (zinc-finger motif), MBT (malignant brain tumour domain), C-HLX (C-terminal EP400 helix formed by residues 2511-2523), bromo (acetyl-lysine binding bromodomain), MRG, (MORF-related gene domain).

a

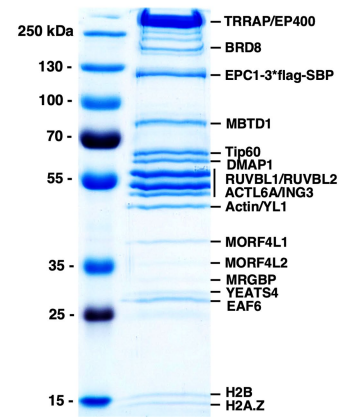

b

Acession	Description	#PSMs	# AAs	NSAF (PSM/AA)	NSAF Norm. to EPC1
Q9Y4A5	TRRAP	3407	3859	0,88	1,16
Q96L91	EP400	1907	3159	0,60	0,80
Q9Y265	RUVBL1	981	456	2,15	2,83
Q9Y230	RUVBL2	959	463	2,07	2,73
Q9H2F5	EPC1	635	836	0,76	1,00
O96019	ACL6A	491	429	1,15	1,51
Q9H0E9	BRD8	436	1235	0,35	0,46
P60709	Actin	1050	375	2,80	3,69
Q9NPF5	DMAP1	337	467	0,72	0,95
Q92993	TIP60	300	513	0,59	0,77
Q9NXR8	ING3	291	418	0,70	0,92
Q05BQ5	MBTD1	305	628	0,49	0,64
Q15906	YL1/VPS72	160	364	0,44	0,58
Q9UBU8	MORF4L1	170	362	0,47	0,62
O95619	YEATS4	165	227	0,73	0,96
Q15014	MORF4L2	111	288	0,39	0,51
Q9NV56	MRGBP	102	204	0,50	0,66
Q9HAF1	EAF6/MEAF6	93	191	0,49	0,64
Q5QNW6	H2B	254	252	1,01	1,33
Q71UI9	H2AZ	46	128	0,36	0,48
P07437	Tubulin	673	445	1,51	1,99
Q70SY1	CREB3L2	60	502	0,12	0,16
Q562R1	ACTBL2	82	376	0,22	0,29
Q16777	H2A	17	129	0,13	0,17

c

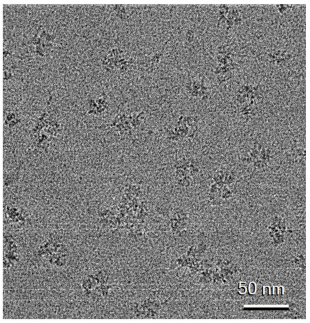

Extended Data Fig. 2 | Biochemical characterization of TIP60-C. a, Colloidal Coomassie blue stained SDS–PAGE analysis of the TIP60-C complex purified using a 3Flag-SBP-tagged EPC1 subunit. **b**, Proteomic analysis of the purified TIP60-C complexes. For each identified protein subunit, the table shows the peptide spectrum matches (PSM) counts, the number of residues, the PSM values normalized by subunit length (NSAFs) and, as an estimate of the stoichiometry, the NSAF value normalized to tagged EPC1. Note that the table indicates that the third ARP in TIP60-C is either actin or ACTL6A. Values were averaged over 3 experiments. **c**, Raw cryo-EM image of purified TIP60-C.

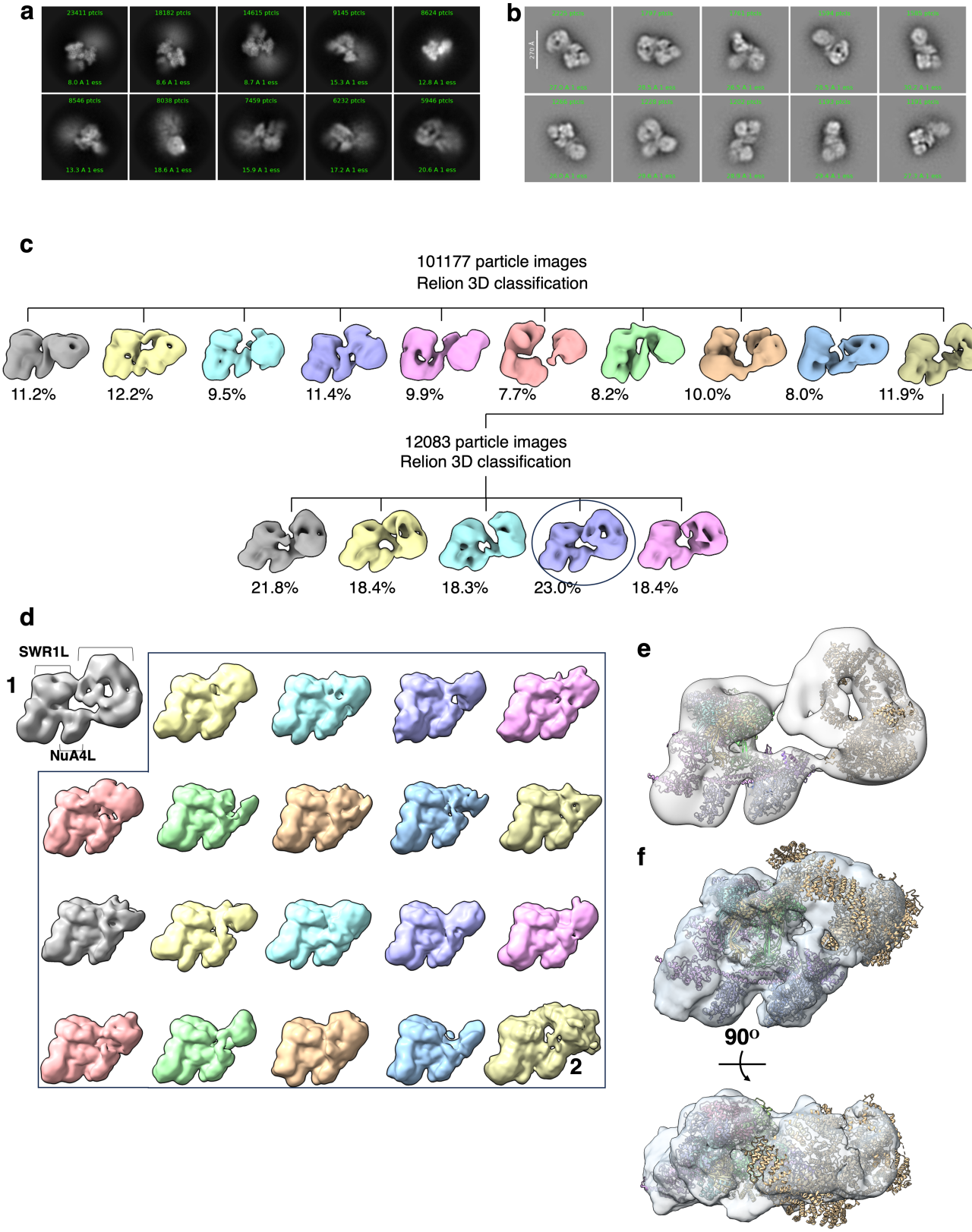

Extended Data Fig. 3 | See next page for caption.

Extended Data Fig. 3 | Structural characterization of TIP60-C. **a**, Characteristic 2D class averages obtained after CryoSPARC image classification. **b**, Characteristic 2D class averages obtained from classification of the negative stained dataset of TIP60-C. c, 3D classification chart of the negative stain dataset of Tip60-C. The class chosen for fit is highlighted with a circle. **d**, Major 3D class average obtained from the negative stained dataset of TIP60-C, designated as 1, and 19 representative OPUS-DSD[44] 3D class averages of the cryo dataset showing the flexible attachment of the TRRAP module to the SWR1L and NuA4L parts of TIP60-C. **e**, Fitting of holo-TIP60-C, including TRRAP, into a 3D class average from negative stained analysis. **f**, Representative OPUS-DSD[44] 3D class average with an additional density at similar location as in the negative stain class. The density next to NuA4L assumes many different orientations both in cryo-EM and negative stain. We chose one orientation, out of many, from cryo-EM to show that this mobile density is big enough to accommodate TRRAP. We show another orientation from negative stain to ascertain that this mobile density corresponds to TRRAP as it shows the distinctive features of TRRAP.

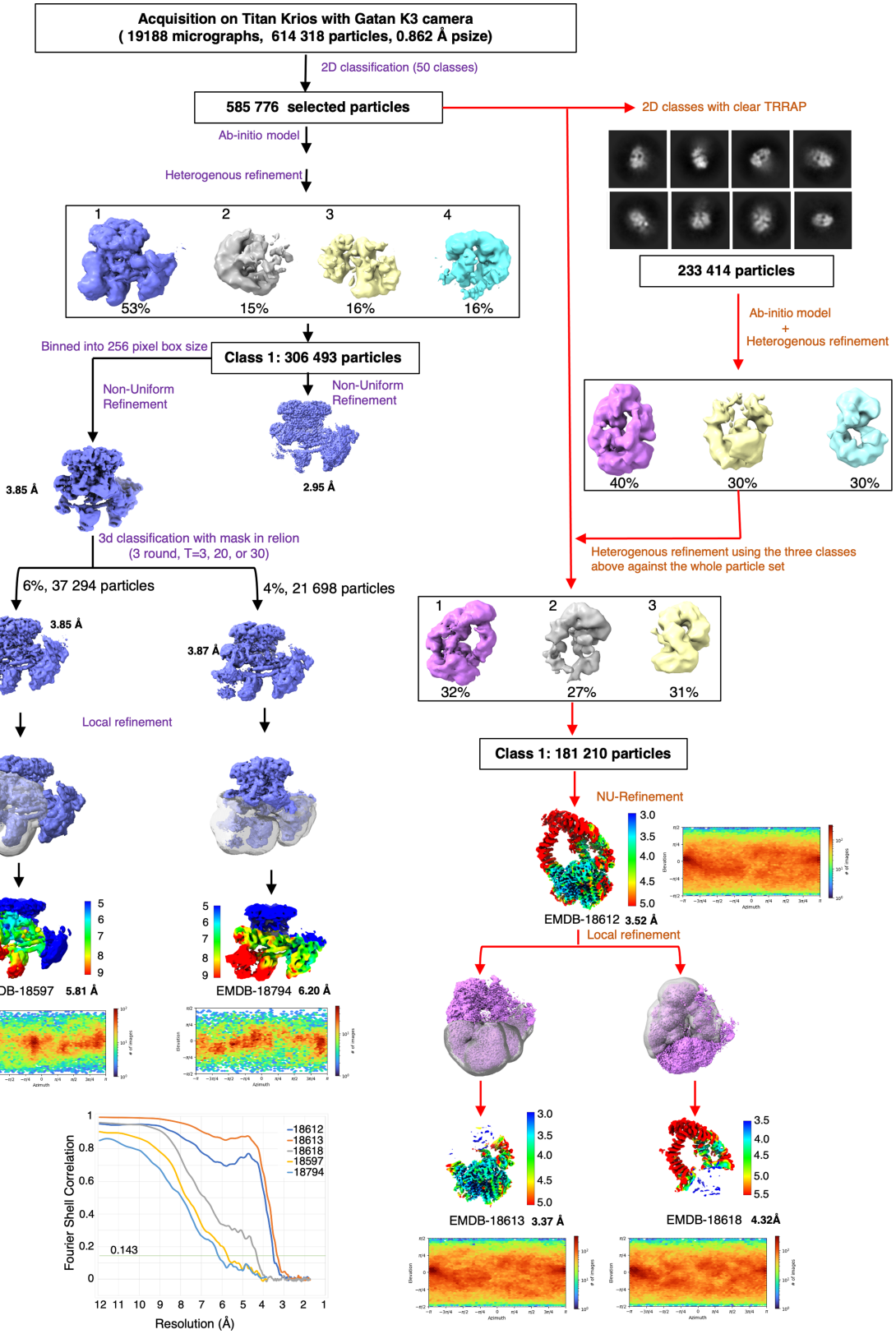

Extended Data Fig. 4 | Cryo-EM data-analysis strategy and resolution assessment for dataset 1. Flow chart illustrating the key image analysis steps that lead to five locally refined maps: Overall refined TRRAP (EMDB-18612), TRRAP base-part refined (EMDB-18613), TRRAP top-part refined (EMDB-18618), Actin - ATPase refined (EMDB-18597) and H2A.Z/H2B map (EMDB-18794). Hollow grey volumes represent the masks used for focused classifications and refinements. Rainbow-coloured maps represent the local resolution of the reconstructions, indicated in Å in the colour bar. FSC curves of all maps are grouped and represented as a function of resolution in angstrom. Viewing direction distribution of the reconstructions are depicted with a colour code from blue to red representing the number of images in each direction.

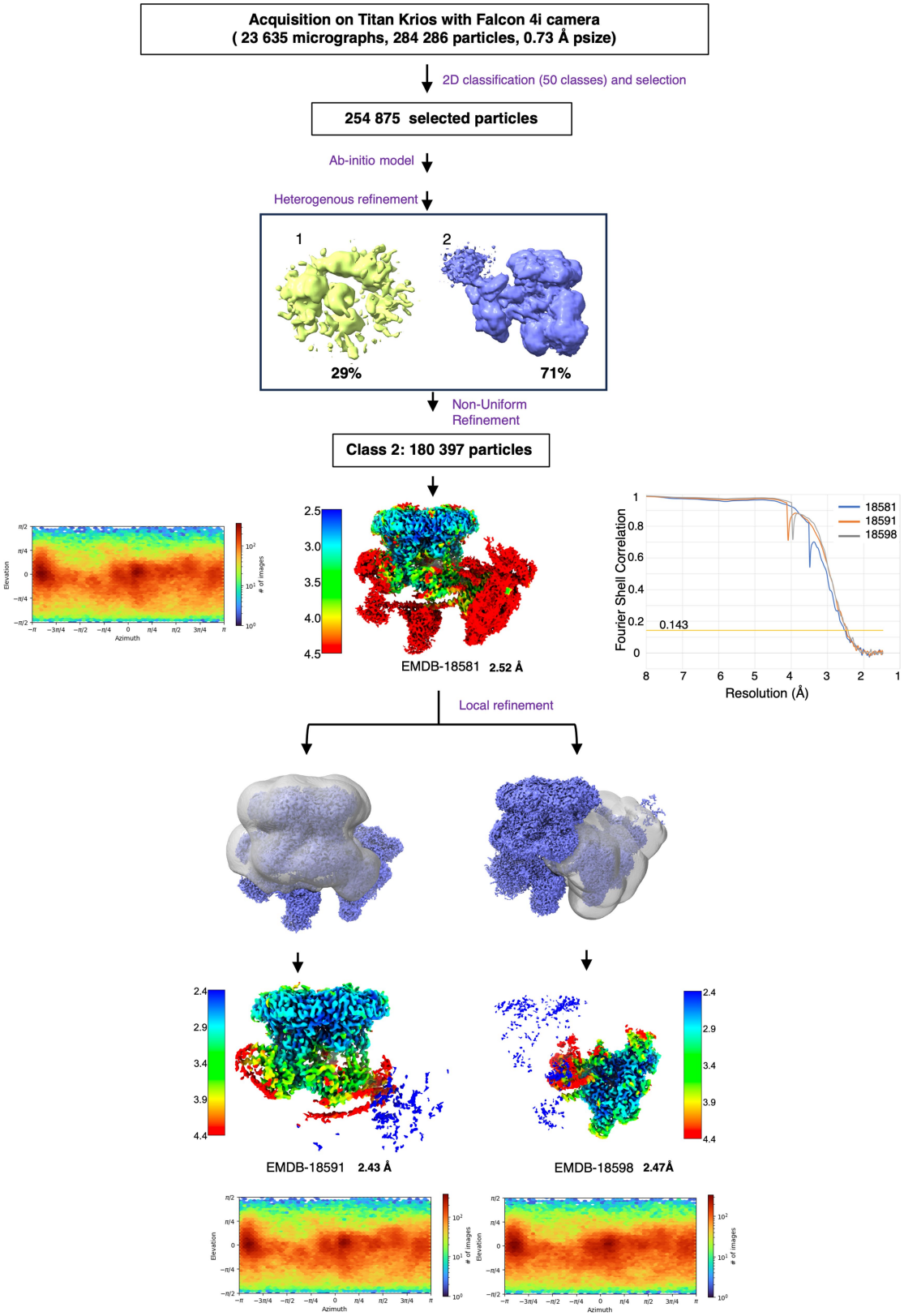

Extended Data Fig. 5 | Cryo-EM data-analysis strategy and resolution assessment for dataset 2. Flow chart illustrating the key image analysis steps that resulted in three locally refined maps with higher resolution: Overall refined TIP60-C (EMDB-18581), RUVB refined (EMDB-18591), and ARP refined (EMDB-18598). Rainbow-coloured maps represent the local resolution of the reconstructions, indicated in Å in the colour bar. FSC curves of all maps are grouped and represented as a function of resolution in angstrom. Viewing direction distribution of the reconstructions are depicted with a colour code from blue to red representing the number of images in each direction.

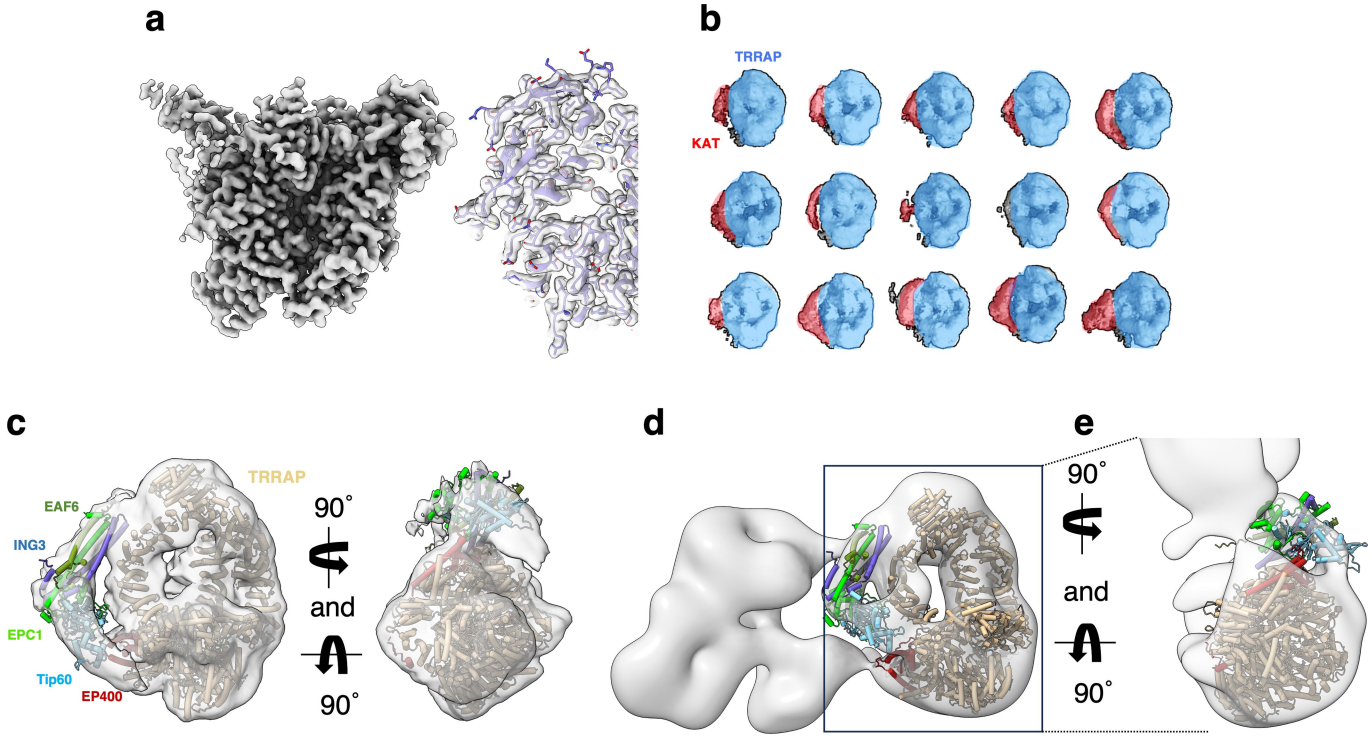

Extended Data Fig. 6 | NuA4L high-resolution features and localization of the flexible KAT module. a, High-resolution features in the local refinement map focusing on NuA4L. **b**, Representative cryoDRGN 3D class averages of a sub-population of the TRRAP module showing a flexible domain (red) contacting the TRRAP subunit (blue). **c**, Docking of an AlphaFold model of the enzymatic KAT module into the TRRAP module obtained from the cryo dataset analysis. The AlphaFold-multimer model generated[47] is highly homologous to the yeast KAT module (PDB: 5J9U)[53]. **d**, Docking of the AlphaFold model of the enzymatic KAT module into the TRRAP module obtained from the negative stain dataset analysis. **e**, Enlarged and rotated view of the docking in **d**.

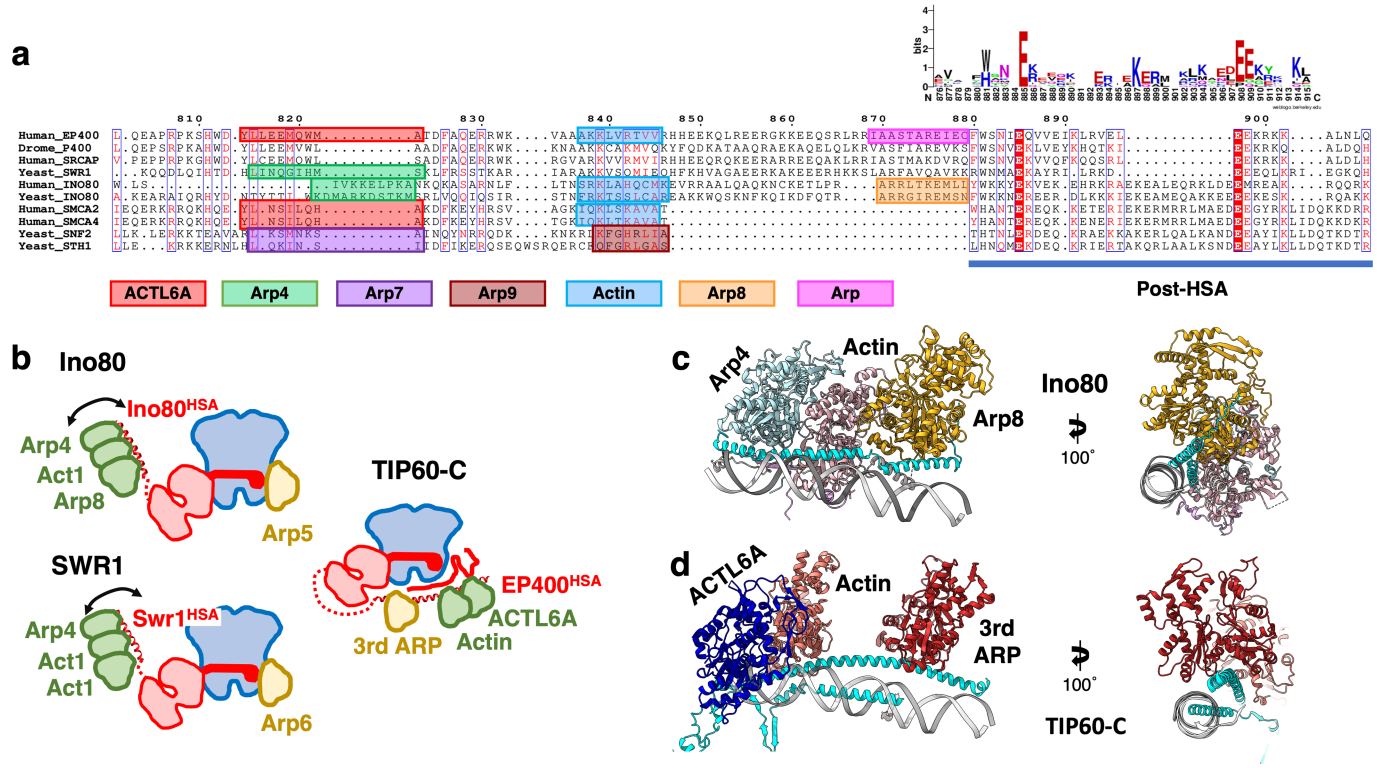

Extended Data Fig. 7 | Position of the HSA helix and spread of the ARPs. **a**, Sequence alignment of the HSA helix found in the ATPase subunit of major chromatin remodeller classes: EP400, SRCAP, SWR1, INO80, SMARCA4, Snf2 and Sth1. ARP-binding sites along the HSA helices are derived from the corresponding atomic models, when available. The Post-HSA motif is highlighted and a conservation profile is shown. **b**, Schematic representation showing the relative positions of the HSA helices, the HSA-bound ARP molecules (green), the hetero-hexameric RuvBL1/RuvBL2 assembly (blue), the ATPase (red) and the ARP grip (yellow) in the INO80, SWR1 and TIP60-C complexes. Double-headed arrows indicate the flexibility of the HSA helix. **c**, Position of the ARP molecules and extranucleosomal long DNA linker in INO80 (PDB 8A5A). **d**, Distribution of the ARP molecules in TIP60-C. DNA was simulated according to **c**. The counter-helix sterically prevents DNA binding to the HSA.

Extended Data Table 1 | Cryo-EM data collection, refinement and validation statistics

	#1 Titan-K3 (EMD-18612,18613,18618,18619,18794) (PDB 8QRI)					#2 Titan-Falcon4 (EMD-18581,18591,18597,18598,18611) (PDB 8QR1)				
Data collection and processing										
Magnification	105000					165000				
Voltage (kV)	300					300				
Electron exposure (e–/Å^2)	52					41				
Defocus range (μm)	1.4-3.5									
Pixel size (Å)	0.862					0.73				
Symmetry imposed	C1					C1				
Initial particle images (no.)	461,262					284,286				
EMD-	18612	18613	18618	18619	18794	18581	18591	18598	18611	18597
Final particle images (no.)	181,210				21,698	180,397				37,294
Map resolution (Å) FSC 0.143	3.52	3.37	4.32	3.5	6.2	2.52	2.43	2.48	2.4	5.81
Map resolution range (Å)	3.0-8.9	3.0-8.9	3.6-8.7	3.0-8.9	4.2-13.6	1.6-7.5	1.6-7.8	2.3-8.2	1.6-8.2	5.0-13.1
Refinement	8QRI					8QR1				
Initial model used (PDB code)										
Model resolution (Å) FSC 0.5	3.8					2.9				
Model composition Non-hydrogen atoms. Protein residues	27,204 3380					39,353 5031				
***B* factors (Å^2)** Protein	162.38					146.44				
R.m.s. deviations Bond lengths (Å) Bond angles (°)	0.004 0.993					0.007 1.221				
Validation MolProbity score Clashscore Poor rotamers (%)	1.87 7.8 0.2					1.09 1.14 0.66				
Ramachandran plot Favored (%) Allowed (%) Disallowed (%)	93.11 6.8 0.09					96.09 3.63 0.28				

nature portfolio

Corresponding author(s): Adam Ben-Shem

Last updated by author(s): Aug 1, 2024

Reporting Summary

Nature Portfolio wishes to improve the reproducibility of the work that we publish. This form provides structure for consistency and transparency in reporting. For further information on Nature Portfolio policies, see our Editorial Policies and the Editorial Policy Checklist.

Statistics

For all statistical analyses, confirm that the following items are present in the figure legend, table legend, main text, or Methods section.

n/a	Confirmed
☐	☒ The exact sample size (*n*) for each experimental group/condition, given as a discrete number and unit of measurement
☐	☒ A statement on whether measurements were taken from distinct samples or whether the same sample was measured repeatedly
☒	☐ The statistical test(s) used AND whether they are one- or two-sided *Only common tests should be described solely by name; describe more complex techniques in the Methods section.*
☒	☐ A description of all covariates tested
☒	☐ A description of any assumptions or corrections, such as tests of normality and adjustment for multiple comparisons
☒	☐ A full description of the statistical parameters including central tendency (e.g. means) or other basic estimates (e.g. regression coefficient) AND variation (e.g. standard deviation) or associated estimates of uncertainty (e.g. confidence intervals)
☒	☐ For null hypothesis testing, the test statistic (e.g. *F*, *t*, *r*) with confidence intervals, effect sizes, degrees of freedom and *P* value noted *Give P values as exact values whenever suitable.*
☒	☐ For Bayesian analysis, information on the choice of priors and Markov chain Monte Carlo settings
☒	☐ For hierarchical and complex designs, identification of the appropriate level for tests and full reporting of outcomes
☒	☐ Estimates of effect sizes (e.g. Cohen's *d*, Pearson's *r*), indicating how they were calculated

Our web collection on statistics for biologists contains articles on many of the points above.

Software and code

Policy information about availability of computer code

Data collection	serialEM 3.7
Data analysis	crYOLO v1.5, Relion v3.1, CryoSPARC2 v3.3.2 and v4.0.0, Coot v0.87, RaptorX v1.02, Chimera v1.14, ChimeraX v1.6.1, Warp v1.0.9, cryoDRGN v1.0, OPUS-DSD v1.0, ADP-EM v2.2, Alphafold v2.2.1, Phenix v1.19.2, Isolde v1.6

For manuscripts utilizing custom algorithms or software that are central to the research but not yet described in published literature, software must be made available to editors and reviewers. We strongly encourage code deposition in a community repository (e.g. GitHub). See the Nature Portfolio guidelines for submitting code & software for further information.

Data

Policy information about availability of data

All manuscripts must include a data availability statement. This statement should provide the following information, where applicable:

- Accession codes, unique identifiers, or web links for publicly available datasets
- A description of any restrictions on data availability
- For clinical datasets or third party data, please ensure that the statement adheres to our policy

Provide your data availability statement here.

Field-specific reporting

Please select the one below that is the best fit for your research. If you are not sure, read the appropriate sections before making your selection.

☒ Life sciences ☐ Behavioural & social sciences ☐ Ecological, evolutionary & environmental sciences

For a reference copy of the document with all sections, see nature.com/documents/nr-reporting-summary-flat.pdf

Life sciences study design

All studies must disclose on these points even when the disclosure is negative.

Sample size	For image analysis sample size (n=614.318) was chosen to assure the possibility to reach highest spatial resolution
Data exclusions	After 2-D classification, images corresponding to false particles or to dammages particles were excluded
Replication	Biochemical experiments were performed in triplicates and all attempts were successfull
Randomization	All particles in the raw images were selected and analysed to ensure a unbiaised initial particle population
Blinding	Image collection was performed automatically without human supervision or selection

Behavioural & social sciences study design

All studies must disclose on these points even when the disclosure is negative.

Study description	*Briefly describe the study type including whether data are quantitative, qualitative, or mixed-methods (e.g. qualitative cross-sectional, quantitative experimental, mixed-methods case study).*
Research sample	*State the research sample (e.g. Harvard university undergraduates, villagers in rural India) and provide relevant demographic information (e.g. age, sex) and indicate whether the sample is representative. Provide a rationale for the study sample chosen. For studies involving existing datasets, please describe the dataset and source.*
Sampling strategy	*Describe the sampling procedure (e.g. random, snowball, stratified, convenience). Describe the statistical methods that were used to predetermine sample size OR if no sample-size calculation was performed, describe how sample sizes were chosen and provide a rationale for why these sample sizes are sufficient. For qualitative data, please indicate whether data saturation was considered, and what criteria were used to decide that no further sampling was needed.*
Data collection	*Provide details about the data collection procedure, including the instruments or devices used to record the data (e.g. pen and paper, computer, eye tracker, video or audio equipment) whether anyone was present besides the participant(s) and the researcher, and whether the researcher was blind to experimental condition and/or the study hypothesis during data collection.*
Timing	*Indicate the start and stop dates of data collection. If there is a gap between collection periods, state the dates for each sample cohort.*
Data exclusions	*If no data were excluded from the analyses, state so OR if data were excluded, provide the exact number of exclusions and the rationale behind them, indicating whether exclusion criteria were pre-established.*
Non-participation	*State how many participants dropped out/declined participation and the reason(s) given OR provide response rate OR state that no participants dropped out/declined participation.*
Randomization	*If participants were not allocated into experimental groups, state so OR describe how participants were allocated to groups, and if allocation was not random, describe how covariates were controlled.*

Ecological, evolutionary & environmental sciences study design

All studies must disclose on these points even when the disclosure is negative.

Study description	*Briefly describe the study. For quantitative data include treatment factors and interactions, design structure (e.g. factorial, nested, hierarchical), nature and number of experimental units and replicates.*
Research sample	*Describe the research sample (e.g. a group of tagged Passer domesticus, all Stenocereus thurberi within Organ Pipe Cactus National Monument), and provide a rationale for the sample choice. When relevant, describe the organism taxa, source, sex, age range and any manipulations. State what population the sample is meant to represent when applicable. For studies involving existing datasets, describe the data and its source.*

Sampling strategy	*Note the sampling procedure. Describe the statistical methods that were used to predetermine sample size OR if no sample-size calculation was performed, describe how sample sizes were chosen and provide a rationale for why these sample sizes are sufficient.*
Data collection	*Describe the data collection procedure, including who recorded the data and how.*
Timing and spatial scale	*Indicate the start and stop dates of data collection, noting the frequency and periodicity of sampling and providing a rationale for these choices. If there is a gap between collection periods, state the dates for each sample cohort. Specify the spatial scale from which the data are taken*
Data exclusions	*If no data were excluded from the analyses, state so OR if data were excluded, describe the exclusions and the rationale behind them, indicating whether exclusion criteria were pre-established.*
Reproducibility	*Describe the measures taken to verify the reproducibility of experimental findings. For each experiment, note whether any attempts to repeat the experiment failed OR state that all attempts to repeat the experiment were successful.*
Randomization	*Describe how samples/organisms/participants were allocated into groups. If allocation was not random, describe how covariates were controlled. If this is not relevant to your study, explain why.*
Blinding	*Describe the extent of blinding used during data acquisition and analysis. If blinding was not possible, describe why OR explain why blinding was not relevant to your study.*

Did the study involve field work? ☐ Yes ☐ No

Field work, collection and transport

Field conditions	*Describe the study conditions for field work, providing relevant parameters (e.g. temperature, rainfall).*
Location	*State the location of the sampling or experiment, providing relevant parameters (e.g. latitude and longitude, elevation, water depth).*
Access & import/export	*Describe the efforts you have made to access habitats and to collect and import/export your samples in a responsible manner and in compliance with local, national and international laws, noting any permits that were obtained (give the name of the issuing authority, the date of issue, and any identifying information).*
Disturbance	*Describe any disturbance caused by the study and how it was minimized.*

Reporting for specific materials, systems and methods

We require information from authors about some types of materials, experimental systems and methods used in many studies. Here, indicate whether each material, system or method listed is relevant to your study. If you are not sure if a list item applies to your research, read the appropriate section before selecting a response.

Materials & experimental systems

n/a	Involved in the study
☐	☐ Antibodies
☐	☐ Eukaryotic cell lines
☐	☐ Palaeontology and archaeology
☐	☐ Animals and other organisms
☐	☐ Human research participants
☐	☐ Clinical data
☐	☐ Dual use research of concern

Methods

n/a	Involved in the study
☐	☐ ChIP-seq
☐	☐ Flow cytometry
☐	☐ MRI-based neuroimaging

Antibodies

Antibodies used	*Describe all antibodies used in the study; as applicable, provide supplier name, catalog number, clone name, and lot number.*
Validation	*Describe the validation of each primary antibody for the species and application, noting any validation statements on the manufacturer's website, relevant citations, antibody profiles in online databases, or data provided in the manuscript.*

Eukaryotic cell lines

Policy information about cell lines

Cell line source(s)	*State the source of each cell line used.*
Authentication	*Describe the authentication procedures for each cell line used OR declare that none of the cell lines used were authenticated.*

Mycoplasma contamination	*Confirm that all cell lines tested negative for mycoplasma contamination OR describe the results of the testing for mycoplasma contamination OR declare that the cell lines were not tested for mycoplasma contamination.*
Commonly misidentified lines (See ICLAC register)	*Name any commonly misidentified cell lines used in the study and provide a rationale for their use.*

Palaeontology and Archaeology

Specimen provenance	*Provide provenance information for specimens and describe permits that were obtained for the work (including the name of the issuing authority, the date of issue, and any identifying information). Permits should encompass collection and, where applicable, export.*
Specimen deposition	*Indicate where the specimens have been deposited to permit free access by other researchers.*
Dating methods	*If new dates are provided, describe how they were obtained (e.g. collection, storage, sample pretreatment and measurement), where they were obtained (i.e. lab name), the calibration program and the protocol for quality assurance OR state that no new dates are provided.*

☐ Tick this box to confirm that the raw and calibrated dates are available in the paper or in Supplementary Information.

Ethics oversight	*Identify the organization(s) that approved or provided guidance on the study protocol, OR state that no ethical approval or guidance was required and explain why not.*

Note that full information on the approval of the study protocol must also be provided in the manuscript.

Animals and other organisms

Policy information about studies involving animals; ARRIVE guidelines recommended for reporting animal research

Laboratory animals	*For laboratory animals, report species, strain, sex and age OR state that the study did not involve laboratory animals.*
Wild animals	*Provide details on animals observed in or captured in the field; report species, sex and age where possible. Describe how animals were caught and transported and what happened to captive animals after the study (if killed, explain why and describe method; if released, say where and when) OR state that the study did not involve wild animals.*
Field-collected samples	*For laboratory work with field-collected samples, describe all relevant parameters such as housing, maintenance, temperature, photoperiod and end-of-experiment protocol OR state that the study did not involve samples collected from the field.*
Ethics oversight	*Identify the organization(s) that approved or provided guidance on the study protocol, OR state that no ethical approval or guidance was required and explain why not.*

Note that full information on the approval of the study protocol must also be provided in the manuscript.

Human research participants

Policy information about studies involving human research participants

Population characteristics	*Describe the covariate-relevant population characteristics of the human research participants (e.g. age, gender, genotypic information, past and current diagnosis and treatment categories). If you filled out the behavioural & social sciences study design questions and have nothing to add here, write "See above."*
Recruitment	*Describe how participants were recruited. Outline any potential self-selection bias or other biases that may be present and how these are likely to impact results.*
Ethics oversight	*Identify the organization(s) that approved the study protocol.*

Note that full information on the approval of the study protocol must also be provided in the manuscript.

Clinical data

Policy information about clinical studies

All manuscripts should comply with the ICMJE guidelines for publication of clinical research and a completed CONSORT checklist must be included with all submissions.

Clinical trial registration	*Provide the trial registration number from ClinicalTrials.gov or an equivalent agency.*
Study protocol	*Note where the full trial protocol can be accessed OR if not available, explain why.*
Data collection	*Describe the settings and locales of data collection, noting the time periods of recruitment and data collection.*
Outcomes	*Describe how you pre-defined primary and secondary outcome measures and how you assessed these measures.*

Dual use research of concern

Policy information about dual use research of concern

Hazards

Could the accidental, deliberate or reckless misuse of agents or technologies generated in the work, or the application of information presented in the manuscript, pose a threat to:

No	Yes	
☒	☐	Public health
☒	☐	National security
☒	☐	Crops and/or livestock
☒	☐	Ecosystems
☒	☐	Any other significant area

Experiments of concern

Does the work involve any of these experiments of concern:

No	Yes	
☒	☐	Demonstrate how to render a vaccine ineffective
☒	☐	Confer resistance to therapeutically useful antibiotics or antiviral agents
☒	☐	Enhance the virulence of a pathogen or render a nonpathogen virulent
☒	☐	Increase transmissibility of a pathogen
☒	☐	Alter the host range of a pathogen
☒	☐	Enable evasion of diagnostic/detection modalities
☒	☐	Enable the weaponization of a biological agent or toxin
☒	☐	Any other potentially harmful combination of experiments and agents

ChIP-seq

Data deposition

☐ Confirm that both raw and final processed data have been deposited in a public database such as GEO.

☐ Confirm that you have deposited or provided access to graph files (e.g. BED files) for the called peaks.

Data access links *May remain private before publication.*	*For "Initial submission" or "Revised version" documents, provide reviewer access links. For your "Final submission" document, provide a link to the deposited data.*
Files in database submission	*Provide a list of all files available in the database submission.*
Genome browser session (e.g. UCSC)	*Provide a link to an anonymized genome browser session for "Initial submission" and "Revised version" documents only, to enable peer review. Write "no longer applicable" for "Final submission" documents.*

Methodology

Replicates	*Describe the experimental replicates, specifying number, type and replicate agreement.*
Sequencing depth	*Describe the sequencing depth for each experiment, providing the total number of reads, uniquely mapped reads, length of reads and whether they were paired- or single-end.*
Antibodies	*Describe the antibodies used for the ChIP-seq experiments; as applicable, provide supplier name, catalog number, clone name, and lot number.*
Peak calling parameters	*Specify the command line program and parameters used for read mapping and peak calling, including the ChIP, control and index files used.*
Data quality	*Describe the methods used to ensure data quality in full detail, including how many peaks are at FDR 5% and above 5-fold enrichment.*
Software	*Describe the software used to collect and analyze the ChIP-seq data. For custom code that has been deposited into a community repository, provide accession details.*

Flow Cytometry

Plots

Confirm that:

☐ The axis labels state the marker and fluorochrome used (e.g. CD4-FITC).

☐ The axis scales are clearly visible. Include numbers along axes only for bottom left plot of group (a 'group' is an analysis of identical markers).

☐ All plots are contour plots with outliers or pseudocolor plots.

☐ A numerical value for number of cells or percentage (with statistics) is provided.

Methodology

Sample preparation	*Describe the sample preparation, detailing the biological source of the cells and any tissue processing steps used.*
Instrument	*Identify the instrument used for data collection, specifying make and model number.*
Software	*Describe the software used to collect and analyze the flow cytometry data. For custom code that has been deposited into a community repository, provide accession details.*
Cell population abundance	*Describe the abundance of the relevant cell populations within post-sort fractions, providing details on the purity of the samples and how it was determined.*
Gating strategy	*Describe the gating strategy used for all relevant experiments, specifying the preliminary FSC/SSC gates of the starting cell population, indicating where boundaries between "positive" and "negative" staining cell populations are defined.*

☐ Tick this box to confirm that a figure exemplifying the gating strategy is provided in the Supplementary Information.

Magnetic resonance imaging

Experimental design

Design type	*Indicate task or resting state; event-related or block design.*
Design specifications	*Specify the number of blocks, trials or experimental units per session and/or subject, and specify the length of each trial or block (if trials are blocked) and interval between trials.*
Behavioral performance measures	*State number and/or type of variables recorded (e.g. correct button press, response time) and what statistics were used to establish that the subjects were performing the task as expected (e.g. mean, range, and/or standard deviation across subjects).*

Acquisition

Imaging type(s)	*Specify: functional, structural, diffusion, perfusion.*
Field strength	*Specify in Tesla*
Sequence & imaging parameters	*Specify the pulse sequence type (gradient echo, spin echo, etc.), imaging type (EPI, spiral, etc.), field of view, matrix size, slice thickness, orientation and TE/TR/flip angle.*
Area of acquisition	*State whether a whole brain scan was used OR define the area of acquisition, describing how the region was determined.*

Diffusion MRI ☐ Used ☐ Not used

Preprocessing

Preprocessing software	*Provide detail on software version and revision number and on specific parameters (model/functions, brain extraction, segmentation, smoothing kernel size, etc.).*
Normalization	*If data were normalized/standardized, describe the approach(es): specify linear or non-linear and define image types used for transformation OR indicate that data were not normalized and explain rationale for lack of normalization.*
Normalization template	*Describe the template used for normalization/transformation, specifying subject space or group standardized space (e.g. original Talairach, MNI305, ICBM152) OR indicate that the data were not normalized.*
Noise and artifact removal	*Describe your procedure(s) for artifact and structured noise removal, specifying motion parameters, tissue signals and physiological signals (heart rate, respiration).*

Volume censoring

Define your software and/or method and criteria for volume censoring, and state the extent of such censoring.

Statistical modeling & inference

Model type and settings

Specify type (mass univariate, multivariate, RSA, predictive, etc.) and describe essential details of the model at the first and second levels (e.g. fixed, random or mixed effects; drift or auto-correlation).

Effect(s) tested

Define precise effect in terms of the task or stimulus conditions instead of psychological concepts and indicate whether ANOVA or factorial designs were used.

Specify type of analysis: ☐ Whole brain ☐ ROI-based ☐ Both

Statistic type for inference
(See Eklund et al. 2016)

Specify voxel-wise or cluster-wise and report all relevant parameters for cluster-wise methods.

Correction

Describe the type of correction and how it is obtained for multiple comparisons (e.g. FWE, FDR, permutation or Monte Carlo).

Models & analysis

n/a	Involved in the study
☐	☐ Functional and/or effective connectivity
☐	☐ Graph analysis
☐	☐ Multivariate modeling or predictive analysis

Functional and/or effective connectivity

Report the measures of dependence used and the model details (e.g. Pearson correlation, partial correlation, mutual information).

Graph analysis

Report the dependent variable and connectivity measure, specifying weighted graph or binarized graph, subject- or group-level, and the global and/or node summaries used (e.g. clustering coefficient, efficiency, etc.).

Multivariate modeling and predictive analysis

Specify independent variables, features extraction and dimension reduction, model, training and evaluation metrics.